PREPARATION AND CHARACTERIZATION OF FORSTERITE AND MEASUREMENT OF ITS DIELECTRIC CONSTANT AND LOSS FACTOR IN THE FREQUENCY RANGE OF 50 Kc/s—25 Mc/s

A Thesis Submitted
in Partial Fulfilment of the Requirements
for the Degree of
MASTER OF TECHNOLOGY

By

PRABHAT KUMAR GHOSH

to the

DEPARTMENT OF METALLURGICAL ENGINEERING
INDIAN INSTITUTE OF TECHNOLOGY, KANPUR

JANUARY, 1979

CERTIFICATE

Certified that the thesis entitled 'Preparation and Characterization of Forsterite and Measurement of its Dielectric Constant and Loss Factor in the Frequency Range of 50 Kc/s - 25 Mc/s' has been carried out under my supervision and has not been submitted elsewhere for a degree.

(A. R. Das)
Professor
Department of Metallurgical Engineering
Indian Institute of Technology,
Kanpur

ACKNOWLEDGEMENTS

With a profound sense of gratitude, I wish to acknowledge Professor A. R. Das under whom this work has come to a successful completion. His lively interest, inspiring guidance, illuminating suggestions and optimistic as well as open minded approach to problems have brought forth this dissertation in the present form.

I owe much to Professor E. C. Subbarao for his interest in this study as well as for his generous permission in allowing me to use his instruments. I am also grateful to Professor D. Chakravorty and Professor D. K. Paul for their active interest in this endeavour.

I acknowledge Mr. B. Sharma, Mr. R. K. Prasad, Mr. Malaviya, Mr. A. K. Singh and Mr. Basak for the assistances rendered by them in the different phases of work. I am grateful to Mr. P. K. Nandi for his immense help.

I am highly indebted to my friends Messrs G. C. Das, A. Sen, H. P. Kaza, P. Sarkar, R. N. Chatterjee, P. Mukherjee, S. Ganguly, S. Dutta, S. N. Paul, N. K. Ghosh and Partha Sarkar who have provided me with their entertaining company during the pastime I had. I shower a lot of hearty thanks on them.

I am thankful to Mr. Bhamra for materialisation of the different schemes into actual experimental apparatus, Mr. V. P. Gupta for accurate tracing of the figures, Mr. Nihal Ahmad for excellent typing the winged manuscript and

Mr. Viswanath for neat ammonia printing and cyclostyling.

I owe a special debt to my parents for their kind understanding and perseverence for this period when I had to keep myself away from them.

Prabhat Kumar Ghosh

CONTENTS

LIST OF TABLES

LIST OF FIGURES

ABSTRACT

Forsterite samples were prepared from pure MgO-SiO_2 and talc-magnesite.. In the talc-magnesite batches, ball clay and $BaCO_3$ were also used as additives. Samples of 2" diameter were prepared and sintered at different temperatures ($1125^{o}C$-$1400^{o}C$) for different times (4½ hrs.-20 hrs.). X-ray analysis was performed for identification of phases. Sintered samples were polished and the measurement of the relative dielectric constant K and the quality factor Q were conducted in the frequency range of 50 Kc/s-25 Mc/s using a Boonton Radio Co. Q-meter Model 260-AP. Both the electroded and unelectroded samples were used in wired and unwired condition. Capacitance cells, which had been used to eliminate extraneous effects were not found helpful and were discarded. Finally the K and Q measurements were done with electroded and wired forsterite samples. For the best sample, made of talc-magnesite and 6.54 percent $BaCO_3$, having a relative density of 0.93, the K and tanδ values were 6.63 and $5x10^{-4}$ respectively and that of pure MgO-SiO_2 with relative density 0.89 had shown K = 5.55 and tanδ = $14x10^{-4}$ Higher density samples had shown higher K and Q values.

CHAPTER 1

INTRODUCTION

For application as high frequency insulation ceramic products are required which are dimensionally stable, have good mechanical strength, and have a low loss factor. Requirements and classification for these materials are indicated in Table 1. Low loss steatite is the most widely used material as it is surpassed for economy in manufacture, because the talc used in the composition is easily pressed and causes the least die wear. The resulting product consists of mainly clinoenstatite in a glassy matrix. Steatite bodies usually come in class L-3 to L-5 of Table 1.

For lower dielectric losses, forsterite ceramics having Mg_2SiO_4 as a main crystalline phase are frequently used. Alkaline earth oxide fluxes are used to give excellent dielectric properties. The high expansion coefficient is detrimental for thermal shock but it is an advantage for forming ceramic-metal seals, since it provides good match for some of the nickel-iron alloys. Table 2 gives typical property descriptions of steatite and forsterite ceramics.

Forsterite has an orthorhombic crystal structure[25,26] with a = 4.76 Å, b = 10.21 Å, c = 5.98 Å and c' = 5.96 Å. It is such that each silicon atom is surrounded by a tetrahedral group of four oxygen atoms and each magnesium is surrounded octahedrally by six oxygen atoms.

In the $MgO-SiO_2$ system, the two stable phases are forsterite (Mg_2SiO_4) and enstatite ($MgSiO_3$), besides periclase (MgO) and silica. The melting point of forsterite is $1890^{o}C$. Forsterite ceramics have been in commercial use in the USA, Europe and Japan.

Navais[1] in a detailed report on a large number of electrical insulators, states that steatite has been the accepted generic name for high-talc containing bodies which in firing develop the mineral clinoenstatite ($MgO \cdot SiO_2$) and some cristobalite. These insulators have been used in large quantities for many radiotransmitter parts during World War II and had good dielectric properties and low Power Factor (~ 0.002) in 300 kc-1mc range with some going as low as 0.0004. Unfortunately they became quite lossy at centimeter and lower wavelengths. In contrast, forsterite composition such as shown in Table 3 maturing at $1250^{o}C$ shows remarkably low losses.

Atlas[2] in his paper reviewed the earlier works on phases of $MgSiO_3$ and mentions the conclusion of the earlier workers Allen, Wright and Clement (1906) that four crystalline modifications, i.e. rhombic enstatite, monoclinic clinoenstatite and two more phases of orthorhombic and monoclinic amphiboles exist. Of these, the only stable phase at all temperatures was enstatite and that the other phases formed metastably below $1100^{o}C$. Atlas in his

investigations, however, showed the existence of two stable phases, i.e. rhombic enstatite occurring upto 985°C and protoenstatite occurring above 985°C upto the point of dissociation into forsterite and liquid. Clinoenstatite was considered to be a low temperature metastable phase formed from protoenstatite by rapid cooling. The transition rhombic enstatite $\rightleftharpoons$ protoenstatite was reconstructive and was accelerated by a flux whereas transformation of protoenstatite to clinoenstatite was displacive.

Thurnauer[3] had discussed forsterite as a low loss material. Zaikina[4] discussed the formation of clinoenstatite phase in the preparation of forsterite from magnesite (58wt%) and quartzite (42wt%) at synthesis temperature range of 1500-1730°C.

Foster[5] made a high temperature X-ray diffraction study of polymorphic inversion of $MgSiO_3$, which though more relevan[t] to steatite formations has also direct connections to forster[ite] formation. According to this scheme, protoenstatite is the stable high temperature phase and clinoenstatite is related to it somewhat as low cristobalite is related to high cristobalite. Foster's scheme of polymorphism and the earlier reported schemes of Bowen and Schairer (1935) and Thilo and Rogge (1939) are shown in Fig. 1 for comparison. Since protoenstatite has a tendency to disintegrate and simultaneously invert to clinoenstatite while standing at

room temperature, the presence of this phase in forsterite porcelains, except in limited amounts is to be avoided. The phase is stabilised against inversion by (a) the presence of a glassy phase in between the protoenstatite crystals or (b) when the protoenstatite crystals are present in very small sizes and the nucleation rate of the clinoenstatite phase is greatly minimised.

From X-ray and microscopic analysis it was found that for the specimens without additives, the formation of forsterite, which was exothermic was found to set in at about 1100°C and complete at 1400°C as shown in Fig. 2.

The formation of protoenstatite began from 1280°C by the secondary reaction of Mg_2SiO_4 and SiO_2. In the specimen with the addition of 5% kaolin (PSF-O) which was sintered at 1460-1500°C, the phases forsterite, protoenstatite, clinoenstatite, α-quartz and periclase, as in Fig. 3 were found. In the specimen with 5% kaolin and 10% $BaCO_3$ (PSF-B) which sintered at 1300-1420°C as in Fig. 4, the phases forsterite, $BaO\cdot SiO_2$, $(BaO)_2(SiO_2)_3$ and BaO glass were found. The dielectric losses at 1 Mc/S of both specimens as in Table 4 were low and at 1 Gc/S the loss of PSF-O was smaller than that of PSF-B.

As practical compositions, the forsterite porcelains were also made from sea water magnesia and sileceous stone instead of from pure $Mg(OH)_2$ and silica. The base composition

was the same as the earlier one, but the additives were $BaCO_3 \cdot ZnO$ and $CaO \cdot (B_2O_3)_2$ glass. The latter were added to the base batch in 5% and 10% by weight and a blank base batch was also made ready. The seven kinds of batches thus prepared were calcined respectively until forsterite forming reaction was completed. They were ground with additional 5% kaolin and fired at various temperatures. It was found that the additives such as $BaCO_3$, ZnO and $CaO(B_2O_3)_2$ glass had a favourable effect of reducing the dielectric loss of the fired specimen, especially the addition of $BaCO_3$ was most effective. However, heating in H_2 at 1300°C showed easy evaporation and reduction and hence for vacuum tube work the additives were not recommended.

Hayami and Ogura[7] studied the kinetics of formation of forsterite from MgO and enstatite and Hayami[8] studied the reverse case of formation of enstatite from forsterite and SiO_2. The first study was of development of forsterite by solid state reaction in mixed powders of MgO and enstatite in various mole ratios in temperature range of 1100-1300°C and times of 100 hrs, followed by quantitative X-ray diffraction measurements. Powders used were coarse particles (10 micron) of one component in a fine grained (one micron) matrix of the other component. The results were shown to agree with Ginstling-Brounstein equation. Reaction rate constants were determined and activation energies in range

of 100-110 kcal/mole were obtained. Fig. 5 shows the G-B function $D(\alpha)$ compared with actual experimental data on forsterite formation.

The second study was similarly of the two component powder system of forsterite and SiO_2 from which enstatite formation was studied. The fit of the G-B function in the second case was not as good. However, the use of functions related to G-B, showed improved fit. The study indicated the development of enstatite on the forsterite as well as the SiO_2 side, suggesting that one MgO of $(2\ MgO)SiO_2$ reacts with SiO_2. Mg is believed to be the main diffusing species. The results of firing in vacuum suggest that the reaction is possibly controlled by the diffusion of Mg^{2+} ion through the enstatite.

Sugiura et al.[9] studied the relation between the microstructure and the electrical and mechanical properties of forsterite. Three kinds of forsterite batches of molar ratio $MgO:SiO_2$ = 2.00:0.82 (M), 2.00:1.00 (F) and 2.00:1.05 (S) were calcined at 1300°C to which 5% kaolin was added. The material was fired to various temperatures. Firing shrinkage, apparent specific gravity, water absorption, dielectric loss, insulation resistance and bending strength of the fired specimen were measured to discuss the relation between the properties and the microstructure.

Above physical properties gave the maximum or minimum values at certain firing temperatures. The specimen M fired at 1550°C, F at 1390°C and S at 1370°C gave the maximum values of firing shrinkage, apparent specific gravity, Te value of volume resistivity, and bending strength and the minimum values of water absorption and dielectric loss. At these maximum or minimum points, each specimen showed a similar microstructure being composed of forsterite crystals of about 10 microns. The texture was dense but was not of the perfect mosaic structure that is obtainable by firing at higher temperatures through the rapid growth of the forsterit crystals. It was suggested that the best composition lay between M and F.

The effect of kaolin addition was studied by Sano et al.[10] The stability of forsterite porcelain at high temperatures in hydrogen atmosphere, which is an applicational requirement, is improved by kaolin. Zero to 10% kaolin was added to forsterite which was prepared from Fukushima siliceous stone and sea-water magnesia in the molar ratio of $MgO:SiO_2$ as 2:1. The temperature range for the sintering of forsterite was extended remarkably by the addition of kaolin and the firing shrinkage was almost constant within this range. The coefficient of linear thermal expansion decreased with the increase of added kaolin, and no significant change was found by repeated heat treatments. With the

addition of 5% kaolin, the dielectric constant and dielectric loss were unvaried and these values were excellent for a high frequency insulator. The result of X-ray diffraction gave only the pattern of forsterite. By microscopic observation the forsterite crystal grains changed from allotromorphic to idiomorphic and glass matrix increased with the kaolin content.

Table 5 gives dielectric properties of specimens fired at different temperatures.

Sugiura et al.[11] studied the relationship between the microstructure and the thermal expansion of forsterite porcelains. The thermal expansion of forsterite porcelain, which is one of the most important properties for use in electron tube, and the effect of different firing temperatures plus that of repeated heating cycles were investigated. The coefficient of linear expansion along each axis of synthesised forsterite were measured by X-ray giving a=10.47, b=12.50 and c=11.05 x 10^{-6} along the respective axis in the temperature range of 20 to 800°C.

Referring to the data of Navais[1] it was pointed out that the elevation of the firing temperature by 25°C would result in an increase of the thermal expansion coefficient by 1.0×10^{-6}, a value considered too high for vacuum sealing purposes with metal. To study this phenomenon many batches of forsterite porcelain were prepared and fired at different

temperatures. The specimens made of talc, sea-water magnesia and $BaCO_3$ showed the marked decrease of the coefficient (about 1×10^{-6}) with the elevation of firing temperature from 1400 to 1500°C. Microscopic observation indicated the increase of glassy phase which has probably the cause of reduction of the expansion coefficient.

The thermal expansion coefficient of specimens containing MgO and SiO_2 in various ratios have also been measured. Forsterite porcelain having excess of SiO_2(SiO_2 47%) showed the increase of the coefficient by about 1.2×10^{-6} by the elevation of the firing temperature from 1400°C to 1600°C. The coefficient however decreased with increase of MgO. The specimens containing excess MgO showed only a small variation. Microscopic observation of the specimens containing excess SiO_2 showed an excessive growth in crystal size of the forsterite when the firing temperature was elevated and the coefficient increased as reported earlier. The samples with excess MgO did not show any grain growth and also the expansion coefficient did not change much.

For a number of compositions, the effect of repeated heatings at lower temperature (1000°C) after firing at higher temperatures, were studied. The results could be classified into two groups. The one in which the coefficient increased and the second group in which it did not change as much. The former had more glass phase under the microscope. The

authors confirmed that the composition of forsterite porcelain for use in electron tube should have excess MgO and the glassy substance should be reduced as far as possible.

Singer and Adolf[12] reported preparation of a forsterite composition matching that of Titanium metal. A prefired mixture of MgO and SiO_2 in the same proportion as in forsterite, together with 15 % clay or 10 % Al_2O_3 gave a ceramic with the required thermal expansion.

A French patent[13] reports the preparation of crystalline $2MgO \cdot SiO_2$ by the low temperature firing of amorphous SiO_2 and MgO. Thus 30-60 % by weight of dry wet-pptd. silica and 40-70 % of MgO was calcined at 900-1000°C [or $Mg(OH)_2/MgCO_3$] and ball milled for 24 hours with water. The mixture was dried at 100°C and sieved (100 mesh). Then 12 % by weight of organic binder (ceresine) was added. The mixture was sieved again and molded at 1000 kg/sq.cm pressure. The compacts are then baked for 1 hr at 1450°C in a continuous kiln so that the material temperature was raised by 75°C/hr to remove organic binder and water. A transluscent crystalline forsterite porcelain is obtained in which the tanδ was 5×10^{-5} while the dielectric loss of the previous ceramic was 2×10^{-3}. The coefficient of thermal expansion of 9.46×10^{-6} could be adjusted to match that of glass by varying SiO_2/MgO ratio. The ceramics were used in radio tubes, condensers and insulators.

General Electric of U.K.[14] reported the production of a forsterite ceramic matching the thermal expansion coefficient of Ti. The material was especially useful for making envelopes of vacuum tubes.

Soga and Anderson[15] determined the thermal expansion coefficient of forsterite upto 1000°C.

Kanchin and Amburz[16] determined $\alpha_{20-1000^\circ C}$ of $(2MgO)SiO_2 = 12.2 \times 10^{-6}$ per deg. °C.

Smoke[17] reviewed 23 years of dielectric research in Rutgers State University describing studies on loss characteristics of forsterite among other insulating ceramic materials.

Russian workers Usov et al.[18-20] reported work on Forsterite and related materials for high frequency applications.

CHAPTER 2

EXPERIMENTAL PROCEDURE

For preparing different types of batches indicated below, the raw materials used were $MgCO_3$, $Mg(OH)_2$, SiO_2, talc and magnesite. In addition, ball clay and $BaCO_3$ were used as additives in one of the batches. Three batch compositions (A) stoichiometric compositions with $MgCO_3$ and SiO_2, (B) Stoichiometric compositions with $Mg(OH)_2$ and SiO_2 and (C) magnesite and talc compositions with additions of ball clay and $BaCO_3$ (listed in table 6) were used.

2.1 Raw Materials

Imported grades of $MgCO_3$, $Mg(OH)_2$, SiO_2 of commercial purity were used. Indigenous grades of talc, magnesite, barium carbonate and an imported grade of ball clay were used. Barium carbonate and unwashed ball clay was used as an additive in batch C. The raw material analysis is given in Table 7.

2.2 Material Preparation

2.2.1 Weighing

Correct proportions of raw materials were weighed out using a single pan digital balance for the preparation of the batches.

2.2.2 Mixing and grinding

All mixing and grinding were done under wet conditions. For grinding of SiO_2, $MgCO_3$, $Mg(OH)_2$, magnesite and talc, high alumina porcelain lined ball mills with alumina balls were used with water as the liquid. Methyl alcohol was used as the liquid for grinding calcined materials containing MgO.

The raw materials of batch numbers A and B were first mixed and ground for 20 hours for good communition of the SiO_2, $MgCO_3$ and $Mg(OH)_2$, particularly the SiO_2. Batch A was then dried and calcined and subsequently reground for 4 hrs in methyl alcohol media. Batch B, after first grinding and drying, was forsterised and subsequently reground in two steps since the material had become considerably hard. Firstly, it was ground in a steel pestel and mortar and deironed. Subsequently, it was ground in pot mill for 8 hrs in water. For processing of Batch C material, firstly the magnesite lumps were crushed in steel pestel, deironed and ground in ball mill for 24 hours in water. The minus 325 mesh powder was taken after wet sieving, dried and mixed with talc for 4 hrs in a pot mill. After drying the additions of ball clay and $BaCO_3$ was made to make up the compositions shown in table 8 and mixed for 4 hours in pot mill, to obtain the final compositions. All drying was done in a temperature controlled electric oven.

2.2.3 Calcination and forsterization

Calcination was done in silicon carbide heated pot type furnace, the materials being kept in hard fired alumina crucibles. The materials were introduced cold and the temperature was brought to the calcination temperature in 6-7 hours. Batch A and B were calcined for 4 hrs at 1000°C, and batch C was calcined for 20 hours at 1150°C. The higher time and temperature was used for batch C as the ground raw material for this was substantially coarser.

Subsequent to calcination the batch B material was also forsterised at 1355°C for 20 hours and reground as noted earlier.

The powder density of the above forsterised material was determined by pycnometer.

2.3 X-ray Powder Diffraction

In order to find out the extent of transformation and formation of phases during calcination and forsterisation, powder patterns of calcined powders were taken using GE XRD-6 type diffractometer with CuK_α radiation.

2.4 Sample Preparation

Samples of all batch materials were prepared for electrical property measurements. The powdered material was mixed with approximately 2% by wt. of P.V.A. and the powder was

pressed into discs of 5 cm diameter using a hand press at a load of 15000 lbs using a cast iron die. For industrial purposes, 5000 psi is reasonable. Pellets of 0.5 cm diameter were also made for trial runs and also for X-ray analysis.

2.5 Sintering

Sintering was done in the pot furnace for the lower temperatures (below 1250°C). A tube furnace and a big box furnace were used for attaining higher temperatures (upto 1400°C). All the three furnaces were silicon carbide heated. Temperatures were controlled by an L and N on-off type controller in conjunction with an oil cooled variac. Temperatures were separately measured with Pt and Pt plus 10% Rh thermocouples and a potentiometer.

Maximum sintering temperatures possible were determined for different batch materials in trial runs so that no sticking occurred between the disc and the substrates as well as in between the discs. Different types of coarse prefired powders, i.e. alumina, zirconia, magnesia, zircon-sand, silica, calcined mixture of magnesia and silica, soft and hard fired forsterite compositions, and fired coarse powders of the components of batch C were used. The best powders were those of hard fired materials of the same composition as the discs. A few samples were sintered at higher temperatures where sticking had occurred. This was done to obtain a very high density. These samples were separated by a diamond

cutter. For the substrates, alumina discs with a layer of coarse powder noted above were used.

Sintering for batches B and C were done in two steps, i.e. first they were presintered at a lower temperature and then finally sintered to different temperatures and times. Batch A material was sintered in one step to different times and temperatures.

Trial runs for presintering and sintering were taken for all batches to determine degree of densification, hardness (for polishability) and sticking propensities.

During presintering runs and low temperature sintering which was done in the pot furnace, the samples were covered by saggers made of alumina. For higher temperatures, saggers could not be used as the diameter of horizontal tube furnace and height of the box furnace were low.

Batch A was fired for different times and temperatures as shown in table 9. For batch B, small 3/8" dia pellets were placed in the tube furnace at such positions, determined by a profile measurement, which gave temperatures of 739, 946, 1067, 1112, 1151 and 1180 degrees centigrade. They were sintered for 15 hrs and the temperature of 1112°C was selected for presintering after examining the characteristics of the corresponding pellets for its polishability. The presintering temperature of 1125°C and time of 15 hrs was chosen for batch B.

Using the above mentioned procedure, the presintering temperature and time for batch C was determined to be 1100°C and 4½ hrs respectively. The final sintering temperature and times for batch C were 1150 and 1200°C for 5 hrs. Samples of batch A were sintered at different temperatures (1260, 1280, 1300, 1380 and 1400°C) for different times (5, 10, 11 and 20 hours). Batch B was studied under presintered condition. Batches C_1, C_2, C_3, C_4 were fired at 1150°C and 1200°C for 5 hours after presintering at 1100°C for 4½ hrs and subsequent polishing. To obtain highly dense samples batch C_3 was also fired at 1160, 1180, 1200 and 1220°C for 10 hrs.

2.6 Polishing

After firing, the discs were polished in a fabricated polishing holder (ref. 23, fig. 6), using a glass plate and 100 mesh and 200 mesh powders (SiC). **At first, one surface was** polished by hand. The polished side was fixed to the holder with a hardenable resin and the second side was polished down to the required thickness. The sample was removed by treatment with acetone. One sample was polished by 600 mesh powder. Polished samples, were stored in a desicator after washing in acetone and oven drying.

2.7 Sample Density

Density was determined by geometrical measurements and weighment using a micrometer and balance respectively. Percent

theoretical density was calculated on the basis of theoretical forsterite density (3.2 gms/cc). Approximate density of each batch was also found out using 'mixture rule' and was denoted as calculated density.

2.8 Water Absorption

The standard method of test for water absorption (ASTM Designation C373-56) was followed to determine the water absorption of the samples. The water absorption (A) which is expressed as a percentage is given by, $A = \frac{W-D}{D} \times 100$; where D and W are the dry weight and the saturated weight of the sample respectively.

2.9 Electroding and Wiring

Four types of electroding were used (i) silver paint, (ii) silver paste, (iii) vacuum deposited aluminum and (iv) aluminum foil. Samples were painted/pasted on both sides. Baking at 150°C in oven was necessary for continuity. It was found that optimum baking time was required to remove all solvent, develop continuity and give minimum values of contact resistance as indicated by the Q-values of the samples. Insulated copper wires, with their insulations stripped were fixed on painted surfaces and further coat of paint was applied for establishing continuity between surface and wires. The wires were held in position by spots of araldite. In some cases coaxial lead wires were joined to these wires.

The painted samples, henceforth termed as electroded samples, are shown in Fig. 6. Some measurements of electroded samples were directly made between parallel plates without wiring.

2.10 Measuring Methods and Elimination of Errors

The measurement of dielectric constant and Q-factor was done on type 260-AP, Boonton Radio Co. Q-meter in the frequency range of 50 Kc/s to 25 Mc/s. The instrument is basically a resonant circuit from which the values of Q and capacitance of the unknown sample can be directly read on a meter and a dial respectively.

The parallel connection method was used. In this case, the circuit was first resonated, using a type 590-A (Boonton Radio Co.) standard coil of known capacitance, to establish reference values Q_1 and C_1. The circuit was reresonated with the unknown forsterite capacitor connected to CAP terminals (fig. 7) and standard coil in its original position. The altered value of Q_2 and C_2 were noted and the actual values of K and Q of the material were calculated as follows:

$$K = \frac{(C_2 - C_1)\ t}{A\varepsilon_0} \qquad (1)$$

$$Q = \frac{(C_2 - C_1)\ Q_1Q_2}{C_1\ (Q_1 - Q_2)} \qquad (2)$$

where t and A are the thickness and area of the capacitor respectively and ε_0 is the permittivity of vacuum.

During measurement of K and Q it has been noted that different type of errors were entering into the results. To eliminate these, measuring methods were subsequently changed. Also to check whether any apparently invisible errors had been introduced or not, variations were done. These errors and their elimination are discussed here along with variation in measuring methods.

(i) Electrode baking conditions

If the silver paint which is used to electrode the sample is not properly baked the sample under test shows low Q and high K values. Thus the presence of solvent obstructs in getting the actual inherent material property (i.e., K and Q).

To remove this, baking time was varied. The sample was kept in electrically heated oven at a particular temperature for different lengths of time.

(ii) Lead length variation and electrical shieldings

Electroded samples with leads were used first for measurement of K and Q. Lead length was varied to see whether there is any effect of lead length on K and Q.

Measurements were also done by electrically shielding the samples by putting the sample in a completely closed aluminium box. Electrical shielding of the lead was done by using coaxial wire. Shielding was done to remove any extraneous effect on sample which is found at high frequencies.

Measurements were taken using shield both in grounded and ungrounded condition.

(iii) Number of leads

The contact resistance has a prominent role in finding out actual Q and K of the material. Use of multiple leads should increase contact area and thereby ensure low contact resistance and at the same time reduce contact inductance effect. This is why measurements were taken using multiple leads though extra capacitance is introduced by its use.

(iv) Fringe effect

Fringe effect was taken care of in micrometer methods (described later) at later stages using guardrings which was grounded. Measurements were also taken using guardring having the same potential as that of lower electrode.

If the test specimen and guard electrode extend beyond the guarded electrode by at least twice the thickness of the specimen and the guard-gap is very small, the field distribution in the guarded area will be identical with that existing when vacuum is the dielectric. Furthermore, the field between the active electrodes is defined and the capacitance can be calculated with the accuracy limited only by the accuracy with which the dimensions are known.

(v) Porosity

Samples used for measurements were not completely dense,

i.e. they did not possess zero porosity. We could not reach zero porosity because of firing problems. It is evident that porous material will show a low K value.[27]

If some moisture is in adsorbed state in the pores it will show a lower value of Q. For this the samples were always kept in a desicator and also plastic bagged during measurement.

To see whether there is any difference in K and Q values between electroded and unelectroded samples, both of them were used. Reliability of micrometer set up was checked using air.

(vi) Thickness variation

Variation of sample thickness has two effects.

(a) The capacitance (ΔC) of the sample increases with lowering of sample thickness and thus $\frac{\Delta C}{C_1}$ becomes high as C_1 is constant at a particular frequency. From equation (2)

$$Q \;\alpha\; \frac{(C_2 - C_1)}{C_1} \cdot \frac{Q_2}{(Q_1 - Q_2)} \text{ i.e. } Q \;\alpha\; \frac{\Delta C}{C_1} \cdot \frac{Q_2}{\Delta Q}$$

as Q_1 is constant for a particular frequency.

Now, $\frac{Q_2}{\Delta Q}$ must decrease if the ratio $\frac{\Delta C}{C_1}$ is made higher as Q is a material property. This can only be achieved by decrease of the Q_2 value which in turn increases the ΔQ value.

It was found during measurements that some times the reading of ΔQ value demands eye estimation. So, if the ratio

$\frac{\Delta C}{C_1}$ is increased, which can be made close to unity by adjusting frequency, more accurate ΔQ value is obtainable and thus higher accuracy can be achieved.

(b) With decrease in sample thickness the fringe effect decreases and thereby increases the accuracy of the K value measurement.

The different types of measurements performed are listed below.

(a) Lead : The number and length was varied and also coaxial wires were used.

(b) Electrode : Both the electroded (wired and unwired) and unelectroded samples were used. Different types of electrodes used were (i) silver painted, (ii) silver pasted, (iii) vacuum deposited aluminum and (iv) aluminum foil.

(c) Parallel Plates : Both flat and pointed electrodes were used (Fig. 8).

(d) Cell : Capacitance cells were designed in accordance with ASTM standards (D150-65T). The errors caused by the series inductance, capacitance and resistance of the connecting leads at high frequencies are eliminated by this micrometer-electrode method. It accomplishes this by maintaining these inductances, capacitances and resistances relatively constant, regardless whether the test specimen is in or out of the circuit. The specimen, which is either the same size as, or

smaller than, the electrodes is clamped between the elctrodes. It is stated that unless the surfaces of the specimen are lapped or ground very flat, metal foil or its equivalent must be applied to the specimen before it is placed in the electrode system[28].

The arrangement of the ungrounded and unshielded cell is shown in Fig. 9. The experimental variations done in this cell were (i) change of air gap to see fringe effect on the K and Q values and (ii) variation of air gap with unelectroded and electroded sample in series with the gap.

One more capacitance cell (Fig. 10) was designed in which a guard ring was properly placed and complete electrical shielding was ensured (using an aluminium box). Short shielded leads were also used. These were done to minimise extraneous effect. The variations employed were (i) use of only air (ii) use of electroded sample and (iii) use of unelectroded samples.

Measurements were taken with,

(i) Guardring having the same potential as that of lower electrode.

(ii) Unguarded, shield grounded.

(iii) Unguarded, shield ungrounded.

(iv) Guarded, shield grounded

(v) Guarded, shield ungrounded.

(vi) Upper electrode soldered, unguarded, shild grounded.

(vii) Ungrounded, unshielded.

In all these measurements in capacitance cell it was observed that the inherent capacitance of the cell itself had been giving much trouble for finding out the actual K and Q values of the material. To minimise this inherent capacitance a new cell was designed with minimum amount of dielectric material used. The feature of this cell was the same as shown in Fig. 10 with a few differences which were as follows:

(i) Structure was of aluminium plate which itself had acted as a shield.

(ii) Both the lower electrode and the guardring were placed on alumina setters fixed by araldite. This was done to disconnect the lower electrode, and the guardring from the body.

(iii) The diameter of the lower electrode was made smaller than that of the smallest sample. This was done to ensure proper guard action.

(iv) A glass tube was used to insulate the micrometer so that it could not touch the body.

This cell was used in (i) guarded, shield ungrounded, (ii) guarded, shield grounded, (iii) guarded, shield with micrometer cap grounded, and (iv) guarded, shield with micrometer cap ungrounded conditions.

Finally, the measurement with electroded and wired (short single lead) samples were adopted as the extraneous effect was unremovable with cell measurements.

CHAPTER 3

RESULTS AND DISCUSSION

3.1 Processing

3.1.1 Raw materials

The analysis of $MgCO_3$, SiO_2, talc, magnesite and ball clay is given in table 7.

3.1.2 Mixing and grinding

All mixing and grinding was done in a potmill using alumina balls as grinding media. Previous work of Das and Gupta[21] showed that assuming wear conditions with ferrite charge no more severe than empty ball load, the contamination level in the alumina jar was 0.2% per hour. The contamination per 1000 gms balls per hour was 0.484 gm. For our case the contamination will be about 0.25 % of alumina per hour as ball: material ratio was 5:1 in comparison to 4:1 for Das and Gupta's case.

3.1.3 Calcination and forsterization

The object of calcination was to remove CO_2, structural water and any other volatile matter (if present) from the raw materials. During decomposition of the raw materials, the particles would become finer. Finer particles are expected to improve sintering.

Forsterization was done at 1355°C for 20 hours as this was the maximum attainable temperature which was imposed by the inherent limitation of the furnace available at that time. The extent of forsterization will be discussed later (3.2).

3.1.4 Sample preparation

Big samples of 5 cm diameter were pressed at 5,000 psi and small samples of 0.5 cm diameter were pressed at 18,000 psi. The green densities of the samples are shown in tables 8, 9 and 10. The green densities of big samples are found lower than those of small samples. This is because of the lower applied pressure during forming of large samples. The limitation imposed by the press capacity (15,000 lbs) had prevented the use of higher pressure on the large samples. In commercial practice, however, pressure generally does not exceed 5,000 psi.

Among all the small pellets of talc-magnesite composition (table 8), the batch C_2 shows highest green density (1.96 gms/cc) and the batch C_4 shows the lowest (1.63 gms/cc). Packing efficiency increases with increase in number of size fractions, i.e. if 3 size fractions are used in place of 2 size fractions. Both ball clay and $BaCO_3$ were used as additives for making batch C_2 whereas there was no additive for the batch C_4. Number of size fractions being more in the batch C_2 and also higher density of $BaCO_3$ (4.43 gms/cc) had increased the green density. The green density of batch

C_3 is more than C_1 as the density of the additive ($BaCO_3$) which was added to the batch C_3 is higher than that of ball clay (calculated density 3.19 gms/cc) which was added to the batch C_1.

Large samples which were pressed at higher pressure show higher density (table 9).

3.1.5 Sintering

Results of densification and thermal history have been shown in tables 8-13. The densest samples used for electrical measurement possess an average density of 2.97 gms/cc (C_3 composition). These samples were fired at 1180°C for 10 hours. The highest density achieved for batch A is 2.85 gms/cc. It was found for batch C_3 (table 13) that porosity increases with sintering at temperatures higher than 1180°C for 10 hours. Bloating is the probable cause for such a behaviour.

3.2 X-ray Analysis

ASTM DATA CARDS were used for identification of phases present in the sintered samples. Expected phases were listed first and then the standard lines (as taken from ASTM CARD) were matched with the lines which were found from the X-ray diffractogram of the sintered samples. In the pure system of MgO-Al_2O_3-SiO_2 the following main phases can be expected depending on the (a) overall average composition (b) local composition which may vary from the average. The phases are

periclase, forsterite, enstatite, protoenstatite, quartz, cristobalite, tridymite, cordierite, mullite, spinel, sapphirine and corundum. In addition when BaO is present further combination, e.g. barium silicate, barium aluminium silicate, barium magnesium silicate etc. are also possible. Matching was done with all the above phases and all the phases except tridymite, mullite, sapphirine and corundum are found present in the samples.

The thermal history and also densification data (only in table 10) of the samples used for phase identification had already been shown in tables 10 and 11. Stoichiometric $MgO-SiO_2$ and stoichiometric talc-magnesite were used as batch compositions. Talc-magnesite with additives were also used.

Standard lines of forsterite, periclase, protoenstatite, high form of protoenstatite and clinoenstatite are shown in table 14. In table 15, standard lines of enstatite, α-quartz, β-quartz, α-cristobalite and β-cristobalite are shown. Standard lines of low cordierite, magnesium aluminate, barium silicate, barium aluminium silicate and barium magnesium silicate are shown in table 16. In the above four tables only those standard lines are shown which have the intensity greater than 10%. The d values and intensity of three intense lines of 27 compounds are shown in table 17. These compounds are also checked for identification of the unknown phases of the samples of interest.

In tables 18-25, only 6 higher intensity lines of forsterite are shown in A part and the phases identified as different from forsterite are shown in B part. All unidentified lines are shown separately in table 26. Sometime, it happens that a particular line of the X-ray diffractogram matches with standard lines of several phases due to overlap. These overlaps are also present in tables 18-25.

Table 18 shows X-ray diffraction data of stoichiometric talc and magnesite samples fired at 1350°C (E_1) and at 1300°C (E_2) for 10 hours. Forsterite, α-cristobalite and β-cristobalite lines are identified. For sample E_1, lines having d values 3.18, 2.91, 2.88 Å and for samples E_2, 3.17, 2.90, 1.96 Å are matching closely with protoenstatite, enstatite and high form of protoenstatite. It is not possible to say whether these lines are single lines or overlaps. No MgO line is found though high silica phases e.g. enstatite and also cristobalite are present. Complete forsterization at lower temperature is possible only when excess MgO is present.[7,8] Only one line remains unidentified in sample E_1.

Table 19 shows X-ray diffraction of samples made of stoichiometric talc and magnesite and sintered at 1250°C (E_3) and at 1200°C (E_4) for 10 hours. All lines are identified.

Table 20 shows X-ray diffraction analysis of stoichiometric samples of $Mg(OH)_2$ and SiO_2 sintered at 1315°C for 20 hours (F_1) and at 1100°C for 4½ hours (F_4). Forsterite lines are

identified. Some unreacted SiO_2 is visible. Protoenstatite, high protoenstatite and low cordierite and magnesium aluminate are also present in the sample F_4. During grinding, there was Al_2O_3 pick up ($\simeq$6%) which had reacted with MgO and SiO_2 to form cordierite and magnesium aluminate. There was no other source of alumina in the raw materials. Lines of cordierite which have d values 8.50 Å and 8.52 Å with intensity 100 and 95 respectively are absent as we did not scan up to that d value. No aluminate is present in the sample F_1. Alumina which comes during grinding in the potmill is in a very fine form. There is one eutectic point in each of the two triangles formed by cordierite-enstatite-silica and cordierite-enstatite-forsterite at 1345°C and 1360°C respectively. The fine alumina powders which were picked up during grinding and reacted to form cordierite and other aluminates had possibly formed eutectic liquid which had turned to a glassy state during cooling. This is the most probable cause for which there is no trace of alumina in the sample F_1.

Table 21 shows X-ray diffraction analysis of stoichiometric $Mg(OH)_2$ and SiO_2 sintered at 1200°C for 12 hours. Only one line remains unidentified in case of sample F_2 and none for sample F_3. Forsterite lines are identified. Presence of α-quartz, β-cristobalite, protoenstatite, enstatite and high protoenstatite shows intermediate reaction between MgO and SiO_2. Hayami[8] had reported that the rate of reaction

of the systems containing MgO and SiO_2, i.e. MgO-SiO_2, MgO-MgO·SiO_2 and 2MgO·SiO_2-SiO_2, is conceivable to be controlled by the diffusion of Mg through the product layer (s). Therefore to obtain the full stoichiometric compound of 2MgO·SiO_2 higher temperature or longer times are necessary, failing which intermediate phases are expected to be present. Lines having d values 3.02 Å (F_2) and 3.01 Å (F_3) are identifiable as that of low cordierite. Lines of cordierite having d values 8.50 Å and 8.52 Å are not visible as we did not scan upto that d value.

X-ray analysis of two samples G_1 and G_2 which are formed from stoichiometric talc, magnesite with additives and sintered at 1100°C for 4½ hours is shown in table 22. Along with forsterite, α-quartz, α-cristobalite, protoenstatite, enstatite and high protoenstatite are present. Lines having d values 3.05 Å and 2.39 Å of sample G_1 are identified as low cordierite and magnesium aluminate respectively. The same argument as given for sample F_4 is also applicable here to justify the presence of cordierite. Other intense lines of magnesium aluminate which have d values 1.43 Å and 2.01 Å with intensities 100 and 70 respectively have overlapped with the nearest lines of the sample. The line having d value 2.39 Å of sample G_1 is also matching with the corresponding line of gamma alumina; but it was discounted since alumina is quite reactive with forsterite. In sample G_2

seven parts of $BaCO_3$ and four parts ball clay were added during preparation. Barium silicate, barium aluminium silicate and cordierite are present in sample G_2. Other lines of barium silicate and barium aluminium silicate are overlapping with that of forsterite. Alumina which was picked up during grinding and also ball clay were the source of Al_2O_3 during formation of barium aluminium silicate.

X-ray analysis of sample G_3 and G_4 which had been formed from stoichiometric talc, magnesite with additives and sintered at 1100°C for 4½ hours is given in table 23. Periclase line (2.11 Å) is found in sample G_4. In both the samples α-quartz, protoenstatite, enstatite and high protoenstatite are present. Barium silicate, barium magnesium silicate are found in sample G_3. Other lines of barium silicate and barium magnesium silicate are indistinguishable due to overlap. Barium carbonate was added to sample G_3 and had acted as a source of BaO for forming barium compounds. Three lines of sample G_3 remain unidentified. All the lines of sample G_4 are identified. Phases containing alumina are not found in the sample G_4. The explanation given for sample F_1 for the absence of phases containing alumina by formation of glass at 1345°C and 1360°C is not valid here as the sample G_4 was sintered at only 1100°C for 4½ hours.

X-ray diffraction of forsterite composition of stoichiometric talc-magnesite with additives is shown in table 24.

Both the samples H_1 and H_2 were fired at 1200°C for 5 hours. All the lines are identified. Barium magnesium silicate is found present in the sample termed H_2. Few lines are also matching with protoenstatite, enstatite and high protoenstatite. Other intense lines of barium magnesium silicate are indistinguishable due to overlap. No phase containing alumina is present in both the samples H_1 and H_2. The same argument of glass formation as given for sample F_1 is also applicable here. Ball clay being present in both the samples has lowered down the liquid formation temperature. Hence, although the samples H_1 and H_2 were treated at a much lower temperature (1200°C) than that of sample F_1 (1355°C) the glassy phase could have formed in these samples.

X-ray diffraction of sample H_3 and H_4 which were formed from stoichiometric talc-magnesite with additives and were sintered at 1200°C for 5 hours is given in table 25. Periclase is present in both the samples. Sample H_3 shows presence of cordierite and magnesium aluminate. Barium carbonate was added in the sample H_3 as additive. Here the possibility of forming glass from aluminate and cordierite is very less as BaO always acts as a devitrifier. Cordierite is present in sample H_4. Both the samples G_4 and H_4 were prepared from same batch composition (stoichiometric talc-magnesite) and sintered at two different temperatures, viz. 1100°C (G_4) and 1200°C (H_4). Free silica which was present in the samples made of pure material (F_1, F_2, etc.) was absent here as talc and magnesite did not contain any free silica. Perhaps alumina does not react with a silicate so easily as it reacts with free silica. This is the most probable cause for which phases containing alumina was not found in the sample G_4 which was fired at a lower temperature (1100°C). At higher temperature (1200°C) appreciable reaction had taken place and cordierite was formed.

In ref. 6 it is stated that in forsterite samples prepared with $BaCO_3$ additives, enstatite phases disappeared at higher temperatures (Figs. 2, 3 and 4) when compared with those of clay additives. In this experiment, however, sintering was

carried out below 1200°C for 5 hours. Both the lower sintering temperature and different base material (i.e. talc-magnesite as against pure components in ref. 6) may explain this difference of presence of enstatite.

It may be observed that a number of lines which remain unidentified from all the samples are shown in table 26.

3.3 Errors in Electrical Measurements

Measurements of K and Q were performed in different conditions to eliminate possible errors. Q values obtained in these measurements are found lower as compared to the values of similar materials reported in literature.

3.3.1 Electroded and wired sample

Table 27 shows K and Q values of electroded forsterite samples using two connecting leads on each face (Fig. 6). The K values have an average variation of 6%. Though there is a wide scatter of Q values between frequencies, it has got an increasing trend from lower to higher frequencies. Sample I and II have shown before (ref. 22, table 8) higher Q values, ranging from 461-1514. Probably overbaking of silver paint has occurred which has brought down the apparent Q of the material.

3.3.2 Variation of number of leads and lead length

Table 28 shows some difference in Q value with multiple leads over one lead (column 3 and 5). Best Q values are

obtained from multiple lead assembly. Use of one lead shows lowest Q value. Intermediate Q value is obtained when one lead but multiple junction is used. The K values are close to reported data's of forsterite. Later on multiple leads were not used to minimise stray wire capacitance and also for practical problems as written earlier.

Table 29 shows that different lead length do not cause any significant change in Q values. The K values are lower due to low density of the sample (approximately 64% as compared with about 85-89% of sample numbers I to VIII). In later measurements short leads were used to minimise extraneous effect.

Table 30 shows K and Q values of unguarded, electroded and single wired forsterite samples in a frequency range of 55 Kc/S to 8.3 Mc/S. The K and Q values can be taken as constant over the entire frequency range. The average K and Q values are 4.9 and 304 respectively. The percent theoretical density of the sample is low (only 62.5%) which leads to lower K value.

Table 31 shows K and Q values of forsterite samples which were sintered at 1150°C and 1200°C for 5 hours. Effect of different baking time on K and Q values are observed to confirm earlier suspicion that improper baking shows lower Q reading. Silver paint obtained from NPL were used. According to the instruction sheet for this paint, the samples

should be kept at 150°C for 2-3 hours for proper baking. Samples used after 90 minutes baking at 150°C shows higher K and lower Q value than that used after 150 minutes baking at 150°C. Samples of batch C_1, C_2 (fired at 1150°C) and C_4 show low K values (2.7-5.0) which is due to low density of the samples.

More experimental variations that had already been shown and discussed in ref. 23 are not discussed here as either there is no relevance with the final action or those are mere repetition.

3.3.3 Electroded samples between parallel plates

Fig. 8 shows arrangement for clamping electroded samples between parallel conductors which is a standard procedure for measurement of capacitance and dielectric constant of disc samples.

Table 32 shows results of discs between parallel plate and table 33 between clamps with smaller but firm contact. The samples were same wired samples (used before) with contact made directly on electroded faces. Here the reported K values are not the actual k of the material. The capacitance values used for calculation includes another component - air capacitance which was in parallel with the sample. This air capacitance arose from the fact that about 1 cm x 1 cm conductor surface remained bare when the sample was introduced between the parallel conductors.

The area of the sample was about 9 sq.cm and the dielectric constant of the forsterite samples was about 6. The area of the aircapacitor was about 1 sq.cm and dielectric constant 1. For table 32 the thickness of aircapacitor was that of the sample and for table 33 it was about 0.6 cm, i.e. about 3 times larger than that of the sample. Thus the actual K value of the samples will be about 2 % less than the K value shown in table 32 and 0.6 % less for table 33. These set ups were never used in future because of the wide and irregular variation in Q values.

The broad conclusion on above measurements are as follows:

(i) Electroded and wired samples show higher Q than electroded samples clamped between plates or sharp contacts.

(ii) Change of lead length within small limits has no effect on measured Q values.

(iii) Multiple leads improve Q, but need not be used to minimise extraneous effect.

3.3.4 Measurement with capacitance cell

Measurement of K and Q were first taken with an unshielded capacitance cell (fig. 9).

Table 34 shows K and Q values of air when airgap is varying from 0.5 cm to 0.025 cm. An ideal air capacitor should show K value close to unity. Here K approaches to unity with decrease of thickness. This is probably due to

end effects. The end effect depends on (a) the thickness (t) of the capacitor as well as (b) the K of the medium. Higher values of t will increase apparent values of K measured. On the other hand, higher effective values of K will reduce fringe effect. The Q values are high and consistent with that of air which should show high Q. At higher frequencies the effect on K is higher which is not unexpected.

In Ref. 28 it is stated that both unelectroded or electroded sample may be placed in a cell for measurement of capacitance.

Table 35 shows comparison between unelectroded and electroded sample. The K values at each step were not calculated as it was a composite capacitor of air and material. The total capacitance values at each step were available. For the unelectroded sample the Q values went on dropping as the air gap between parallel disc conductors and the disc sample was reduced until it reached a very low value of nearly unity when the sample was touched by the conductor plates. But with an electroded sample the variation of air gap had no effect. This experiment was not reproducible later with another cell and reason for this was also not found.

Table 36 again gives similar comparison. The Q value was unmeasurable when the measurement was taken with the

unelectroded sample in touched condition. The sample with better baked electrodes shows higher Q, although overbaking, as remarked earlier, leads to reduction of the Q value. The same sample was used before (table 30). The K and Q values of the sample with better baked electrodes are comparable with that at 55 Kc/S of table 30. The K value (4.61) is low as the sample was porous (62.5 % theoretical density).

Measurement of ΔC, K and Q values were performed, which had already been reported in ref. 23, table 40 and table 41, with the samples XIII and XIV which were used in tables 35 and 36, after lowering down their thicknesses. The Q values did not vary much as was expected. Thin samples are supposed to give more accurate results as discussed earlier.

The broad conclusion from the unshielded and unguarded cell measurements are:

(1) Unelectroded samples give very low Q value.

(2) Q values of electroded samples when tested in cell are similar to those tested by wiring.

(3) Baking characteristics of electrodes have significant effect on Q values measured.

(4) Higher porosity samples give lower Q values.

Table 37 shows K and Q values of air as measured by the shielded and guarded capacitance cell. Here Q values are very low as compared to Q values of air as found before.

Different conditions are tried. Maximum value of Q is obtained in ungrounded and unshielded condition. From now onwards 'unshielded condition' actually means shielding in unearthed condition. But these values are also much lower compared to the previous results. The probable cause is change of design and higher humidity in August. Previous air capacitance values were taken during dry summer whereas these measurements were taken during monsoon. The K values are also higher as compared to previous values, though the trend is not as high as found before. Here also K is decreasing with decreasing airthickness. Lowering of fringe effect can explain this behaviour.

In table 38, ΔC, the total capacitance of cell and Q are measured. From the data it is clear that with decrease of air thickness capacitance of air does not increase proportionally. It is possible only if the capacitance of the cell itself and that of the circuit have already been introduced in the air capacitance. The capacitance of dielectric is given by: $C = \frac{A}{t} K \varepsilon_0$, where A is the area of the capacitor (dielectric), t is its thickness, ε_0 is the permittivity of a vacuum and K is the relative permittivity of the dielectric. The measured capacitance contain two components, inherent capacitance of the cell C_C, which can be taken as constant and the capacitance of dielectric C_D, which depends on the geometric factor A/t. Let C_T be total

capacitance of the cell consisting of the two components. Then,

$$C_T = C_C + C_D$$
$$= C_C + \frac{A}{t} K \varepsilon_o$$

$\therefore$ If C_T is plotted against A/t, K can be found out from the slope of the straight line provided the above linear relationship is valid.

Fig. 11 shows total capacitance versus A/t plot. From the figure it is seen that the plot is not a straight line but a curve. Here also the slope of the curve at different points is equal to $K\varepsilon_o$. For clarification calculation is given below for 3 points.

Point A : $C_T = 132.7$ pf, $\frac{A}{t} = 745$ cm; $\therefore K = \frac{\text{Slope}}{\varepsilon_o} = \frac{\frac{71}{745}\times 100}{8.854} =$

Point B : $C_T = 80.7$ pf, $\frac{A}{t} = 353$ cm, $\therefore K = \frac{\frac{46.8}{353}\times 100}{8.854} = 1.5$

Point C : $C_T = 27.3$ pf, $\frac{A}{t} = 18$ cm, $\therefore K = \frac{\frac{2.6}{18}\times 100}{8.854} = 1.6$

It is clear that more accurate value of K is obtained at lower thickness. In the above consideration the fringe effect, has not been taken into account. The fringe effect, which is higher for greater thickness of the capacitor, leads to higher K value for thicker air capacitor than the thin one. In early measurements (Table 31) the same observation, i.e. increase of K value with increase of capacitor thickness was found.

Table 39 shows ΔC the net capacitance of cell and Q value of air using capacitance cell. For all the conditions the trend of Q value is same. Q is decreasing with increase in air gap as was seen in earlier measurements. As ΔC has not increased proportionally as gap is decreased, surely some inherent capacitance of the cell and that of the circuit are present. This capacitance value should be deducted from the ΔC value during calculation of K of air. The same procedure as adopted for the previous experiment is also applicable here for elimination of extraneous effect, i.e. by plotting total C versus A/t and taking K from the slope of the curve. The ΔC value is always higher in shielded condition than that in unshielded condition. It points out that inherent capacitance is higher in shielded condition. Use of pinconductor (Fig. 10) has not changed the C or Q value to a large extent. The assembly with shield in unearthed condition gives lower K value and external effect is less. In standard coils also the shields are not earthed. In ref. 28 it is stated that the shield can also be connected with the guardring which is earthed. The above two statements are anomalous. In the capacitance cell (1690 A) which is used for lower frequency and is a standard spare for the Boonton Q meter, the shield is earthed. According to the measurements performed it can be stated that assembly with shield earthed should not be used for high frequencies.

In table 40, K and Q values of unelectroded, unguarded forsterite sample are given. The K value is closer to the expected value ($\simeq 6$) in shielded condition. The Q value is decreasing with decrease in air thickness. In Q values a peak at 0.300 cm is seen. It points out that only one mechanism (either series or parallel inherent capacitance) is not active. In arrangement 2B, $\Delta C:C_1$ ratio was made high by adjusting frequency. Increase in ΔQ value occurs at such condition for balancing the increase in $\Delta C:C_1$, ratio and this ΔQ is more reliable than that in arrangement 2A. It must be noted that in previous experiments very low Q values were obtained when unelectroded samples were used in touched condition. But here the Q values are appreciable. The K values are taken only in touched condition as in other positions of the conductor plate it was forming a composite capacitor of air and the disc sample.

In the measurements as described in table 39 and table 40 guardring was not used as the guardring was not helpful in the earlier measurements. For a proper guarded condition the sample diameter should be greater than that of lower electrode which should be surrounded by guardring. The samples used earlier was smaller than lower electrode which was surrounded by guardring.

To minimise the inherent cell capacitance and also to make an effective guardring a new cell was designed. The

cell being made of metal (aluminium) acts also as a shielded cell but without having any dielectric material inside. Measurements of K and Q of forsterite samples were taken in this cell in four different conditions. Table 41 shows that the Q values are low. The K values are much higher than the expected and the K value increases sharply with increase in sample thickness. Fringe effect increases with the increase in sample thickness and thereby increases the apparent K of the material. The inherent capacitance of the cell itself is also higher which has brought the apparent K value higher.

The cell was originally designed to avoid external influences for which minimum amount of dielectric material was used. But the external influence which had unexplainably increased the K value was much higher than the previous cells. So, cell measurements were discarded and electroded and wired method was again adopted.

3.4 Data on K and Q Measurements

The reported K and Q values of forsterite vary from 6-11.5 and 500-10,000 respectively [1,3,6,10]. Both the K and Q value should remain constant in a frequency range upto 10,000 Mc/S as discussed in Appendix II. Peak in tanδ may be observed only at very high frequency which is beyond the range of the Q meter.

For porous samples it is expected that both the K[27] and Q[9] values should be lower than the reported values of samples which were completely dense.

The average K and Q values obtained for the densest sample (93 % theoretical) made of stoichiometric talc-magnesite with 7 parts of $BaCO_3$ additive are 6.63 and 2074 respectively in frequency range of 100 Kc/S-25 Mc/S. For pure forsterite samples of 89 % theoretical density the average values of K and Q obtained are 5.55 and 707 respectively. The lower K and Q value is attributable to the lower density of the samples. Sintering of pure forsterite samples at temperature higher than 1400°C for obtaining denser material was not possible because of limitation imposed by the furnace available.

The effect of a particular additive towards the K and Q value was not observable because to attain that objective, the sample should have equal and high densities or else the effect of density and additives would not be separable.

Table 42 shows the average K values of 3 batches fired to different densities. The K value remains constant within the frequency range 70 Kc/S to 11 Mc/S. The K value is higher for higher density samples. During calculation of average K value, the thin samples were only taken into account as it is the thin samples which show more accurate K values.

Table 43 shows K and Q values of electroded and wired forsterite samples. Measurement was done at 6 different frequencies. The variation of the K value with the change of density cannot be predicted here as there is a wide scatter in values ranging from 5.08-7.48. Literature values, as reported earlier, shows higher Q values for higher density samples. Here also the densest material made of talc-magnesite and $BaCO_3$ shows higher average Q values (2074) than that of lower density material (616). Though the variation in percent calculated density is not much, the above trend is confirmed from water absorption values, which show distinctly that lowest absorption sample give highest Q values. For pure material with 1.07 percent water absorption, the average Q value is 707. So, it can be predicted that samples with zero absorption will show higher Q values than those found in the table.

Table 44 shows the K values of electroded and wired samples with varying thickness. Thicker samples always show higher K values. At high frequencies thicker samples had shown lower K values at some cases (Table 31). The cause of such drop is not understandable. The K values of the samples have been plotted against the sample thicknesses (Fig. 12). There is a flattening trend of the plot at lower thickness. The thin sample shows closer expected K value than that of thick one. The flattening trend and the closer expected K value for thin samples were also observed in Table 31.

Higher apparent K values (6.53-8.39) were observed in earlier measurements (Tables 27 and 28). This was mainly due to under baking and also due to high thickness of the samples. Q values were low in all the earlier measurements (section 3.3) as the porosity of the samples were high. Porous samples also show a lower K value.

CHAPTER 4

CONCLUSIONS

(1) Samples of zero porosity is necessary to achieve optimum properties. To achieve zero porosity higher firing temperature is required since longer grinding time is not possible if contamination is to be avoided.

(2) For complete forsterization higher reaction temperature is necessary.

(3) Thin samples with well baked and wired (short) electrodes will give accurate value of dielectric constant, K.

(4) The K values obtained are fairly close to literature. Higher values also have been reported in literature.

(5) The values of $\tan\delta \times 10^4$ obtained (5-20) are higher than that of the reported (1-15) in literature. Superior values of $\tan\delta$ can be expected with samples of high density.

(6) The loss factor ($K \tan\delta$) obtained (0.003) for the best sample meets the requirement necessary for insulating ceramics of grade L-6.

CHAPTER 5

SUGGESTIONS FOR FURTHER WORK

(1) The powder characteristics, pressing condition, sintering time and the temperature can be investigated in order to obtain optimum densification for particular raw materials.

(2) The effect of different additives may be investigated by obtaining a base material of zero porosity.

(3) The relationship between microstructure and electrical properties (K and Q values) can be established.

(4) Other properties of forsterite, e.g. thermal expansion, thermal conductivity etc. may be investigated.

(5) Electrical measurements in the microwave region should be done.

In fact, a programme is already underway to investigate (4) and (5).

TABLE 1

Jan-I-10 Minimum Requirements for Insulating Ceramics, Radio Class L

Porosity:

No liquid penetration at 10,000 psi pressure.

Thermal Stress Resistance:

Type A - withstand 20 cycles from 100°C into 0°C water.

Type B - withstand 5 cycles from 100°C into 0°C water.

Transverse Strength:

Greater than 3000 psi.

Dielectric Strength:

Greater than 180 volts/mil.

Dielectric Constant:

Less than 12 after 48 hr water immersion.

Loss factor ($k' \tan\delta$):

Grade L-1 $<$ 0.150

L-2 $<$ 0.070

L-3 $<$ 0.035

L-4 $<$ 0.016

L-5 $<$ 0.008

L-6 $<$ 0.004.

TABLE 2

Typical Properties of Steatite and Forsterite

Typical Applications Properties	Steatite H.F. Insulation Electrical appliance insulation	Forsterite H.F. Insulation ceramic-to metal seals
Density (g/cm^3)	2.5-2.7	2.7-2.9$^{\varphi}$
Water absorption ( )	0.0	0.0
Coefficient of linear thermal expansion/^{o}C	8.6-10.5x10^{-6}	11 x 10^{-6}
Safe Operating temp ^{o}C	1000-1100	1000-1100
Thermal Conductivity ($cal/cm^2/cm/sec/^{o}C$)	0.005-0.006	0.005-0.01
Tensile strength (psi)	8000-10000	10000-15000
Compressive strength (psi)	65000-130,000	60000-100,000
Flexural strength (psi)	16000-24000	18000-20000
Impact strength (ft-lb;$\frac{1}{2}$" rod)	0.3-0.4	0.03-0.04
Modulus of elasticity (psi)	13-15 x 10^6	13-15 x 10^6
Thermal shock resistance	Moderate	Poor
Dielectric strength (volts/mil; 1/4" thick)	200-350	200-300
Resistivity (ohms-cm)$^{\varphi}$	10^{13}-10^{15}	10^{13}-10^{15}
Power Factor (1 Mc)	0.0008-0.0035	0.0003
Dielectric constant	5.5-7.5	6.2-6.6

$^{\varphi}$ Theoretical density 3.2 gms/cc.

TABLE 3

Forsterite Composition Maturing Around 1250°C (Cone 10)

Composition No.	166	166E	190-1A	190-1B	190-1C	190-WA	190-2B	190-2C	190-3A	190-3B	190
Sierramic talc	84	80	70	60	50	70	60	50	60	50	51.8
$Mg(OH)_2$			15	25	35	10	20	30	15	25	33.2
BaF_2	10	10	10	10	10	10	10	10	10	10	10
Kentucky Ball Clay No. 4	3	7				7	7	7	10	10	5
Bentonite	3	3	5	5	5	3	3	3	5	5	
	100	100	100	100	100	100	100	100	100	100	100
Fired in air (tunnelkiln) Cone	10	10	10	10	10	10	10	10	10	10	10
Water absorption percent	0	0	0	0	3.35	0	0	0	0.1	0	0.9
3 cm wavelength K	6.15	6.30	6.34	6.11	-	6.39	6.35	6.29	-	-	6.34
PF x 10^{-4}	15	20	9	6	-	4	5	5	-	-	163

(After Ref. 1 Table XXII.)

TABLE 4

Dielectric Properties at High Frequencies (After Ref. 6, table 3)

No.	1 Mc/s $\tan\delta \times 10^4$	ε	10,000 Mc/s $\tan\delta \times 10^4$	ε
PSF-O	3	6	6	6
PSF-B	1	6	12	6

TABLE 5

Dielectric Properties of Samples of Stoichiometric Forsterite Plus Additions of Different Percentage of Korean Kaolin: FK-0 (F 100 K 0), FK-1 (F 97.5 K 2.5), FK-2 (F 95 K 5), FK-3 (F 92.5 K 7.5) and FK-4 (F 90 K 10). (After Ref. 10, Table 6)

Specimen	ε and tanδ	$(\times 10^{-4})$	Firing temp. of specimens (°C) 1370	1400	1450	1500	1550	1610
FK-0	ε	50 KC/S		6.6	7.6	7.9	8.4	11.5
		1 MC/S		7.2	8.0	8.2	8.2	11.2
	tanδ	50 MC/S		13	1	1	3	1
		1 MC/S		3	1	2	2	2
FK-1	ε	50 KC/S	7.6	7.6	7.6	8.1		
		1 MC/S	7.6	7.6	7.7	8.0		
	tanδ	50 KC/S	1	1	1	1		
		1 MC/S	1	1	1	1		
FK-2	ε	50 KC/S	7.7	8.0	7.8	8.1		
		1 MC/S	7.8	8.0	8.0	7.0		
	tanδ	50 KC/S	1	1	1	1		
		1 MC/S	2	2	2	2		
FK-3	ε	50 KC/S	7.5		7.3	7.5		
		1 MC/S	7.5		7.7	7.4		
	tanδ	50 MC/S	6		4	5		
		1 MC/S	6		3	5		
FK-4	ε	50 KC/S	7.3	7.9	7.4	7.0		
		1 MC/S	7.9	8.0	7.5	7.6		
	tanδ	50 KC/S	9	6	1	5		
		1 MC/S	6	9	2	6		

TABLE 6

Composition of Various Batches of Forsterite

Batch		Ingredients
A	$MgCO_3 + SiO_2$	Stoichiometric*
B	$Mg(OH)_2 + SiO_2$	Stoichiometric*
C	Talc+Magnesite	Stoichiometric*

*Stoichiometric means $MgO : SiO_2 :: 2:1$.

TABLE 7

Analysis of $MgCO_3$, SiO_2, Talc, Magnesite and Ball Clay

Constituents	$MgCO_3$	SiO_2	Talc	Magnesite	Ball Clay
MgO	42.65	Nil	34.00	47.54	Trace
SiO_2	0.79	94.50	57.66	0.77	62.06
CaO	0.42	1.04	1.46	1.64	Trace
Al_2O_3			1.16	Nil	21.38
Fe_2O_3	1.40	6.00	2.84	1.60	7.20
TiO_2			Nil	Nil	Nil
Na_2O and K_2O	Nil	Nil	Nil	Nil	8.68
L.O.I.	54.94	-	1.22	50.80	-

TABLE 8

Progressive Densification Data for Different Forsterite Batches of Stoichiometric Talc-Magnesite Composition

Composition in parts: Calcined stoichiometric mixture of talc and magnesite	Ball clay	$BaCO_3$	Batch No.	Sample No.	Actual Temp. °C	Time Hrs.	Average Green density gms/cc	Fired density gms/cc	Percent theoretical density	Percent calculated density
100	4	0	C_1	1	1277	4½	1.83	2.94	92	89
				2	1265	"		2.89	90	87
				3	1227	"		2.90	91	87
				4	1084	"		1.88	59	57
				5	878	"		1.75	55	53
100	4	7	C_2	1	1277	"	1.96	3.01	94	89
				2	1265	"		2.98	93	88
				3	1227	"		2.98	93	88
				4	1084	"		2.11	66	62
				5	878	"		1.94	61	57
100	0	7	C_3	1	1277	"	1.95	3.02	94	89
				2	1265	"		3.01	94	89
				3	1227	"		3.00	94	88
				4	1084	"		2.12	66	62
				5	878	"		1.95	61	57
100	0	0	C_4	1	1180	"	1.63	2.97	93	89
				2	1151	"		2.84	89	85
				3	1112	"		1.99	62	60
				4	1067	"		1.98	62	59
				5	946	"		1.89	59	57

Pressure applied = 18,000 psi.

TABLE 9

Densification and Thermal History of the Forsterite Samples Used for Electrical Measurements

Batch No.	Sample No.	Pressure used psi	Actual Temp °C	Time in Hrs.	Thick-ness in cm	Dia-meter in cm	Average Green density gms/cc	Average fired density gms/cc	Average percent theore-tical density	Average percent calculated density
A+	I	5,000	1380	11	0.201	3.535	1.01	2.84	89	88
	II		1380	11	0.205	3.535				
	V		1280	5	0.199	3.603	1.01	2.71	85	84
	VI		1280	5	0.212	3.596				
	IV	8,000	1260	20	0.199	3.552	1.28	2.85	89	88
	VII		1300	20	0.197	3.532	1.28	2.75	86	85
	VIII		1300	20	0.211	3.503				
B*	XI	4,000	1125	15	0.163	4.743	1.43	2.06	64	64
C_2	XIII		1100	$4\frac{1}{2}$	0.221	4.432	1.46	2.00	63	59
	XIV		1100	$4\frac{1}{2}$	0.116^{φ}	4.432				

+First calcined at 1000°C for 4 hours.

*First forsterized at 1355°C for 20 hours.

$^{\varphi}$Later on this thickness was brought down to 0.0724 cm.

TABLE 11

Thermal History and Composition of Forsterite Samples Used for X-ray Diffraction

Sample No.	Composition	Temp. °C	Time Hrs.	Pressure applied psi
F_1	B	1355	20	
F_2	B	1100	$4\frac{1}{2}$	
F_3	B	1200	12	
F_4	B	1200	12	
G_1	C_1	1100	$4\frac{1}{2}$	5000
G_2	C_2	"	"	
G_3	C_3	"	"	
G_4	C_4	"	"	
H_1	C_1	1200	5	
H_2	C_2	"	"	
H_3	C_3	"	"	
H_4	C_4	"	"	

TABLE 12

Densification Data and Thermal History of Forsterite Samples of Stoichiometric Talc-Magnesite Composition with Additives Used for Electrical Measurements

Batch No.	Sample No.	Temp. °C	Time hrs	Average thick-ness, cm	Average diameter, cm	Average Fired density, gms/cc	Average percent theoretical density	Average percent calculated density
1	2	3	4	5	6	7	8	9
C_1	1	1150	5	0.052	4.336	2.44	76	73
	2	"	"	0.085	4.336			
	3	"	"	0.107	4.363			
	4	"	"	0.597	4.374			
	1	1200	5	0.079	4.035	3.02	94	91
	2	"	"	0.078	4.034			
	3	"	"	0.111	4.025			
	4	"	"	0.544	4.046			
C_2	1	1150	5	0.043	4.531	2.05	64	60
	2	"	"	0.104	4.540			
	3	"	"	0.111	4.544			
	4	"	"	0.248	4.543			
	1	1200	5	0.070	4.097	2.73	85	81
	2	"	"	0.092	4.097			
	3	"	"	0.062	4.107			
	4	"	"	0.402	4.124			

...Contd.

Table 12 (...Contd.)

1	2	3	4	5	6	7	8	9
C_3	1	1150	5	0.107	4.037			
	2	"	"	0.105	4.026	2.89	90	85
	3	"	"	0.115	4.010			
	4	"	"	0.405	4.030			
	1	1200	5	0.057	3.985			
	2	"	"	0.061	3.962	2.90	91	85
	3	"	"	0.054	3.979			
	4	"	"	0.477	3.982			
C_4	1	1150	5	0.047	4.873			
	2	"	"	0.057	4.881	1.36	43	41
	3	"	"	0.044	4.879			
	4	"	"	0.290	4.894			
	1	1200	5	0.053	4.617			
	2	"	"	0.085	4.630	1.98	62	59
	3	"	"	0.093	4.625			
	4	"	"	0.394	4.629			

Pressure applied = 5,000 psi.

TABLE 13

Densification Data and Thermal History of Forsterite Samples of Stoichiometric Talc-Magnesite Composition with $BaCO_3$ Additive and also of Stoichiometric $MgCO_3$-SiO_2 Used for Electrical Measurements

Batch No.	Sample No.	Temp. °C	Time hrs	Average thickness cm	Average Diameter cm	Fired density gms/cc	Average percent theoretical density	Average percent calculated density	Average percent water absorption
C_3	1	1160	10	0.5152	4.0938	2.91	91	86	0.99
	2	1180	10	0.5464	4.0854	2.98	93	87	0.14
	3	1180	10	0.5376	4.0902	2.96			
	4	1200	10	0.5168	4.0868	2.96	92	87	0.20
	5	1200	10	0.5178	4.0856	2.96			
	6	1220	10	0.4812	4.0724	2.94	92	87	0.50
	7	1220	10	0.5058	4.0976	2.96			
A	PM1	1400	10	0.5250	3.9172	2.85	89	88	1.07
	PM2	1400	10	0.5070	3.9024	2.86			
	PM3	1400	10	0.5248	3.8824	2.84			
	PM4	1400	10	0.4972	3.9130	2.85			

Pressure applied = 5,000 psi

TABLE 14

ASTM X-ray Data for Forsterite, Periclase, Protoenstatite, Protoenstatite (high form) and Clinoenstatite

Forsterite		Periclase		Protoenstatite		Protoensta-tite (high form		Clinoensta-tite	
dÅ	I/I_o	dÅ	I/I_o	dÅ	I/I_o	dÅ	I/I_o	dÅ	I/I_o
5.110	26	2.106	100	3.16	100	3.240	20	4.4130	12
3.880	69	1.489	52	2.97	20	3.170	100	3.2867	50
3.730	25	1.216	12	2.90	40	2.908	40	3.1743	60
3.487	21	0.9419	17	2.87	20	2.726	20	2.9795	95
3.000	17	0.8600	15	2.72	20	2.551	30	1.8783	100
2.768	53			2.54	40	2.305	20	2.5418	35
2.513	73			2.29	20	1.975	20	2.5238	35
2.458	100			1.96	60	1.968	20	2.4594	60
2.268	59			1.71	20	1.716	13	2.4358	20
2.250	33			1.63	40	1.642	20	2.3793	16
2.161	15			1.49	60	1.499	15	2.2186	20
1.748	60			1.37	20	1.495	15	2.2080	20
1.670	13			1.31	40			2.1399	12
1.636	12			1.26	20			2.1190	45
1.618	15							2.1150	45
1.497	27							1.7874	12
1.479	30							1.7648	12
1.396	12							1.7626	12
1.351	17							1.7333	12

TABLE 15

ASTM X-ray Data for Enstatite, α-Quartz, β-Quartz, α-Cristobalite and β-Cristobalite

Enstatite		α-Quartz		β-Quartz		α-Cristobalite		β-Cristobalite	
dÅ	I/I_o	dÅ	I/I_o	dÅ	I/I_o	dÅ	I/I_o	dÅ	I/I_o
4.410	14	4.260	35	4.34	20	4.04	100	4.15	100
3.303	35	3.343	100	3.40	100	3.138	12	2.53	80
3.167	100	2.458	12			2.845	14	2.07	30
2.941	45	2.282	12			2.489	18	1.641	60
2.872	85	1.817	17					1.460	50
2.825	25	1.541	15					1.380	20
2.706	25	1.375	11					1.266	30
2.534	45							1.210	30
2.494	50							1.131	20
2.471	30								
2.114	25								
2.096	20								
2.058	14								
1.984	14								
1.958	25								
1.603	20								
1.520	14								
1.485	35								
1.470	20								

TABLE 16

ASTM X-ray Data for Low Cordierite, Magnesium Aluminate, Barium Silicate, Barium Aluminium Silicate and Barium Magnesium Silicate

Low Cordierite		Magnesium Aluminate		Barium Silicate		Barium Aluminium Silicate		Barium Magnesium Silicate	
d Å	I/I_o	d Å	I/I_o	d Å	I/I_o	d Å	I/I_o	d Å	I/I_o
8.52	95	2.43	90	6.95	20	6.39	40	4.04	20
8.45	100	2.01	70	3.746	100	4.57	20	3.75	30
4.91	30	1.43	100	3.669	60	3.77	30	3.54	100
4.67	14			3.299	50	3.44	60	3.34	50
4.09	50			3.249	55	3.33	70	3.28	40
3.381	50			3.123	30	3.24	70	3.19	20
3.369	40			3.120	30	3.00	70	3.836	20
3.149	25			2.794	16	2.901	40	3.711	20
3.132	55			2.780	40	2.758	50	3.655	40
3.039	65			2.756	35	2.574	100	3.601	30
3.035	65			2.343	20	2.406	30	2.514	40
3.012	55			2.267	45	2.316	30	2.364	30
2.650	20			2.221	20	2.263	20	2.264	20
2.644	20			2.199	16	2.167	100	2.197	30
2.637	12			2.132	90	1.994	20	2.157	30
2.334	12			2.080	16	1.946	20	2.114	30
2.107	12			2.076	18	1.801	50	1.928	20
2.102	12			1.975	12	1.625	20	1.826	40
				1.970	18	1.576	20	1.607	30
				1.911	14	1.455	50	1.586	30
				1.874	12	1.428	60		

TABLE 17

ASTM X-ray Data of Compounds Used for Identification of Unknown Phases

Name	Formula	d Å	Intensity
Mullite syn*	$3Al_2O_3 \cdot 2SiO_2$	3.39-3.43-2.21	100-95-60
Barium magnesium silicate	$Ba_3MgSi_2O_8$	2.81-2.93-4.05	100-95-70
Barium magnesium silicate	$Ba_2MgSi_2O_7$	3.17-2.92-1.94	100-55-45
Barium magnesium silicon oxide	$BaMgSiO_4$	3.15-2.63-4.57	100-45-40
Barium silicate	$Ba_2Si_3O_8$	3.79-3.33-3.28	100-87-76
Barium silicate	$Ba_5Si_8O_{21}$	3.26-3.74-3.80	100-90-80
Barium silicate	$Ba_3Si_5O_{13}$	3.85-3.78-3.25	100-80-80
Barium silicate/Sanbornite	$BaSi_2O_5$	3.97-3.09-3.34	100-75-70
Alpha Barium silicate (high temp.)	α-$BaSi_2O_5$	4.05-2.22-3.17	100-80-75
Beta Barium silicate (low temp.)	β-$BaSi_2O_5$	3.09-4.00-3.32	100-95-95
" "	$BaSi_4O_9$	3.49-6.96-2.31	100-80-80
" "	$BaO \cdot 4SiO_2$	3.54-2.91-2.05	100-65-45
Barium magnesium aluminium silicate	$BaMg_2Al_3(Si_9Al_3O_{30})$	7.18-3.23-2.93	100-100-90
Barium aluminate	$Ba_3Al_2O_6$	2.91-4.12-2.06	100-35-25
" "	$BaAl_{12}O_{19}$	2.51-2.79-2.70	100-85-82
" "	$BaAl_2O_4$	3.17-4.56-2.62	100-80-80

Table 17 (...Contd.)

Name	Formula	d Å	Intensity
Barium aluminosilicate		2.48-3.53-3.33	100-70-60
Barium aluminium oxide	$Ba_3Al_2O_6$	2.92-4.13-2.38	100-40-25
Barium aluminium silicate	$Ba_3Al_6Si_2O_{16}$	3.07-3.09-3.52	100-65-50
" " " /Barium feldsper q syn	$BaAl_2Si_2O_8$	3.29-2.97-3.99	100-100-70
" " " /Paracelsian	$BaAl_2Si_2O_8$	4.00-3.30-2.99	100-70-50
" " " /Celsian syn	$BaAl_2Si_2O_8$	3.36-3.48-2.59	100-65-50
" " "	$BaAl_2Si_2O_8$	7.79-1.95-2.97	100-65-50
Magnesium aluminium oxide/spinel syn	$MgAl_2O_4$	2.44-2.02-1.43	100-58-58
Magnesium aluminium silicate/High cordierite syn	$Mg_2Al_4Si_5O_{18}$	8.48-3.03-3.14	100-85-65
" " " /Cordierite	$Mg_2Al_4Si_5O_{18}$	3.13-8.54-8.45	100-80-80
Gamma aluminium oxide/γ alumino syn	γ-Al_2O_3	1.98-1.40-2.39	100-100-80

* syn: synthetic.

TABLE 18

X-ray Diffractogram of Stoichiometric Forsterite Composition With Talc and Magnesite Sintered at 1350°C for 10 hours (E_1) and at 1300°C for 10 hours (E_2) respectively

(A) List of six higher intensity lines of forsterite phase.
(B) List of lines of intensity I/I_o higher than 10 for phases other than forsterite

(A)

E_1			E_2		
d Å	I/I_o	Phase	d Å	I/I_o	Phase
2.47	100	F	2.46	100	F
2.52	90	F	2.51	90	F
2.77	70	F	1.74	75	F
1.75	69	F	2.77	61	F
2.27	60	F	2.27	55	F
3.90	51	F	3.88	49	F
			1.50	49	F

(B)

E_1			E_2		
d Å	I/I_o	Phase	d Å	I/I_o	Phase
4.11	16	βC	4.08	33	αC
3.18	19	P/PH/E	3.17	36	P/PH/E
2.91	12	P/PH/E	2.90	11	P/PH/E
2.88	13	PH/P/E			

TABLE 19

X-ray Diffractogram of Stoichiometric Forsterite Composition with Talc and Magnesite Sintered at 1250°C for 10 hours (E_3) and 1200°C for 10 hours (E_4) respectively.

(A) List of six higher intensity lines of forsterite phase.
(B) List of lines of intensity I/I_o higher than 10 for phases other than forsterite

(A)

E_3			E_4		
d Å	I/I_o	Phase	d Å	I/I_o	Phase
2.46	100	F	2.45	100	F
2.52	84	F	2.51	89	F
2.76	67	F	2.24	69	F
1.75	64	F	1.74	69	F
3.88	54	F	2.76	63	F
2.28	53	F	2.26	51	F

(B)

E_3			E_4		
d Å	I/I_o	Phase	d Å	I/I_o	Phase
3.18	34	P/PH/E	3.17	24	P/PH/E
2.90	29	P/PH/E	2.89	30	P/PH/E

TABLE 20

X-ray Diffraction of Stoichiometric Forsterite Composition with $Mg(OH)_2$ and SiO_2 sintered at 1355°C for 10 Hours and 1100°C for $4\frac{1}{2}$ hours Respectively.

(A) List of six higher intensity lines of forsterite phase.
(B) List of lines of intensity I/I_o higher than 10 for phases other than forsterite.

(A)

F_1			F_4		
d Å	I/I_o	Phase	d Å	I/I_o	Phase
2.46	100	F	2.46	100	F
2.51	82	F	3.34	90	F
2.77	77	F	2.51	80	F
1.75	70	F	2.77	68	F
3.90	65	F	1.75	63	F
2.27	50	F	3.89	57	F
2.25	50	F			

(B)

F_1			F_4		
d Å	I/I_o	Phase	d Å	I/I_o	Phase
			4.29	26	αQ
			3.34	90	αQ
			3.17	20	P/PH/E
			3.08	11	LC
			2.72	29	PH
			2.51	80	βC/F
			2.11	52	M
			1.94	20	F/P/PH
			1.49	51	M/F/P
			1.38	12	MA

TABLE 21

X-ray Diffraction of Stoichiometric Forsterite Composition with $Mg(OH)_2$ and SiO_2 both Sintered at 1200°C for 12 hours.

(A) List of six higher intensity lines of forsterite phase.
(B) List of lines of intensity I/I_0 higher than 10 for phases other than forsterite.

(A)

F_2			F_3		
d Å	I/I_0	Phase	d Å	I/I_0	Phase
2.48	100	F	2.47	100	F
2.53	63	F	2.53	76	F
1.74	61	F	1.75	64	F
2.26	58	F	2.78	59	F
2.79	55	F	3.92	58	F
3.93	50	F	2.27	54	F

(B)

F_2			F_3		
d Å	I/I_0	Phase	d Å	I/I_0	Phase
3.38	22	αQ	4.31	22	αQ
3.20	21	P/PH/E	3.37	83	αQ
3.02	19	LC	3.20	26	P/PH/E
2.48	100	F/M	3.01	27	LC/F
1.50	40	M/F/P	2.90	11	P/PH/E
			2.53	76	βC/F
			1.64	20	βC/F
			1.52	12	P/F
			1.48	42	M/F

TABLE 22

X-ray Diffraction of Stoichiometric Forsterite Composition of Talc, Magnesite with Additives, both Sintered at 1100°C for 4½ hours

(A) List of six higher intensity lines of forsterite phase.
(B) List of lines of intensity I/I_o higher than 10 for phases other than forsterite.

(A)

G_1			G_2		
d Å	I/I_o	Phase	d Å	I/I_o	Phase
2.46	100	F	2.46	100	F
2.51	93	F	2.78	81	F
2.77	68	F	3.90	71	F
1.75	61	F	1.75	69	F
3.88	59	F	2.27	54	F
2.25	49	F	3.90	71	F

(B)

G_1			G_2		
d Å	I/I_o	Phase	d Å	I/I_o	Phase
4.31	12	αQ	4.33	16	αQ
3.30	13	αQ	3.64	21	BS
3.17	45	P/PH/E	3.35	42	αQ
3.05	11	LC	3.30	32	BAS
2.94	17	P/PH	3.18	23	P/PH/E
2.88	34	PH/P/E	3.07	20	LC
2.73	35	PH	2.91	29	P/PH/E
2.39	11	MA	2.73	32	PH
1.49	36	M/F/P	2.60	32	PH
			2.51	95	F/P
			1.62	26	F/P
			1.48	41	F/P
			1.32	16	F/P

TABLE 23

X-ray Diffraction of Stoichiometric Forsterite Composition of Talc, Magnesite with Additives, both Sintered at 1100°C for 4½ hrs.

(A) List of six higher intensity lines of forsterite phase.

(B) List of lines of intensity I/I_o higher than 10 for phases other than forsterite.

(A)

G_3			G_4		
d Å	I/I_o	Phase	d Å	I/I_o	Phase
2.45	100	F	2.45	100	F
2.51	93	F	2.51	83	F
2.77	79	F	1.75	63	F
3.88	73	F	2.76	60	F
1.75	69	F	3.88	55	F
3.48	55	F	2.26	51	F

(B)

G_3			G_4		
d Å	I/I_o	Phase	d Å	I/I_o	Phase
4.31	19	αQ	3.17	37	P/PH/E
3.64	23	BA	2.88	33	p/PH/E
3.56	30	BMS	1.48	41	M/F
3.36	38	αQ			
3.28	29	BMS			
3.18	16	P/PH/E			
2.91	23	P/PH/E			
2.72	33	PH			
2.59	28	PH			

TABLE 24

X-ray Diffraction of Stoichiometric Forsterite Composition of Talc, Magnesite with Additives, both Sintered at 1200°C for 5 hours.

(A) List of six higher intensity lines of forsterite phase.
(B) List of lines of intensity I/I_o higher than 10 for phases other than forsterite.

(A)

H_1			H_2		
d Å	I/I_o	Phase	dÅ	I/I_o	Phase
2.46	100	F	2.46	100	F
2.51	78	F	2.51	74	F
1.75	58	F	2.76	64	F
2.77	55	F	2.25	58	F
3.88	54	F	1.75	52	F
2.25	48	F	3.88	46	F

(B)

H_1			H_2		
d Å	I/I_o	Phase	d Å	I/I_o	Phase
3.18	37	P/PH/E	3.35	36	αQ
2.88	32	P/PH/E	3.27	38	BMS
2.46	100	F/M	3.17	33	P/PH/E
			2.91	34	P/PH/E
			2.58	23	PH
			2.46	100	F/M
			1.94	11	P/F
			1.49	35	M/F/P

TABLE 25

X-ray Diffraction of Stoichiometric Forsterite Composition of Talc, Magnesite with Additives, both Sintered at 1200°C for 5 hours

(A) List of six higher intensity lines of forsterite phase.
(B) List of lines of intensity I/I_o higher than 10 for phases other than forsterite.

(A)

H_3			H_4		
d Å	I/I_o	Phase	d Å	I/I_o	Phase
2.45	100	F	2.47	100	F
2.51	93	F	2.52	73	F
1.74	64	F	2.79	53	F
2.77	61	F	1.75	53	F
2.26	56	F	2.25	49	F
3.87	51	F	1.48	48	F

(B)

H_3			H_4		
d Å	I/I_o	Phase	d Å	I/I_o	Phase
3.33	11	αQ	3.18	44	P/PH/E
3.19	28	P/PH/E	3.02	27	LC
3.06	16	LC	2.89	35	P/PH/E
2.88	66	P/PH/E	2.47	100	F/M
2.45	100	F/M	2.13	12	M
2.10	50	M	1.95	11	P/F
2.04	12	MA			
1.94	12	P/F			
1.49	47	M/F/P			

TABLE 26

Unidentified X-ray Diffraction Lines in Forsterite Compositions

Sample	d Å	I/I_o	Sample	d Å	I/I_o
E_1	3.65	23	G_2	6.56	16
F_1	5.45	16		5.65	10
F_3	1.55	10		4.67	10
F_4	1.38	12		1.46	11
G_1	1.66	11	G_3	6.60	17
				4.67	12
				1.50	46

TABLE 27

Measurement of K and Q of Electroded Forsterite Samples Using Two Connecting Leads on Each Face

Frequency Kc/s	I		II		IV		V		VI	
	K	Q	K	Q	K	Q	K	Q	K	Q
105	7.86	31	7.73	49	7.33	427	6.70	203	6.89	110
200	8.39	34	7.64	63	7.28	1224	6.76	2863	6.92	162
400	7.71	30	7.53	8	6.94	91	6.53	159	6.66	215
800	7.76	50	7.65	46	7.18	559	6.71	515	6.74	350
1500	7.69	193	7.65	149	6.80	88	6.79	874	6.54	1033
2600	7.73	118	7.70	169	7.27	284	6.75	959	6.80	939
6000					7.06	80	6.54	537	6.62	276
11500	7.72	133	7.76	254	7.35	46	6.76	685	6.91	820

TABLE 28

Measurement of K and Q of Unshielded and Electroded Forsterite Sample Using Different Number of Leads and Different Lead Length

Frequency Kc/s	V					
	One lead on each side; lead length 8 cm		5 leads on each side; lead length 5 cm		5 leads on each side but using one lead; Lead length 5 cm	
	K	Q	K	Q	K	Q
5000	7.88	50	7.28	922	8.13	182
6000	7.64	59	6.88	259	8.05	112
7000	7.83	64	7.23	260	8.17	128
8000	7.87	70	7.37	294	8.32	119
9000	7.82	75	7.26	324	8.23	88
10000	7.79	71	7.14	257	8.14	100
11000	7.90	82	7.22	237	8.19	81
12000	8.05	72	7.29	283	8.35	88

TABLE 29

Measurement of K and Q of Unshielded and Electroded Forsterite Sample Using Different Lead Lengths

Frequency Kc/s	XI					
	3" lead		6" lead		12" lead	
	K	Q	K	Q	K	Q
2500	4.62	172	4.53	376	4.65	270
3000	4.49	220	4.56	313	4.63	288
4000	4.55	231	4.60	286	4.80	279
*4200	4.62	206	4.65	285	4.83	235
4200	4.58	224	4.63	282	4.81	273
**4700	4.53	275	4.59	272	4.75	282
5000	4.53	275	4.57	272	4.77	271
5500					4.78	226
5700	4.58	222	4.62	291		
4700	4.55	242	4.56	247	4.78	271
5000	4.54	492	4.51	273	4.74	336
5700	4.44	252	4.50	334	4.74	298
7000	4.44	275	4.58	392	4.86	254
9000	4.56	258	4.64	261	5.00	247
*10000	4.49	229	4.63	212	5.05	177
10000	4.52	223	4.65	214	5.06	167
11000					4.55	144
11200			4.74	222		
11400	4.61	199				

* Frequency switch changed

**Frequency overlap between higher and lower range.

TABLE 30

Measurement of K and Q of Unguarded, Electroded and Wired Forsterite Sample

Frequency Kc/s	XIV	
	K	Q
55	4.85	87
80	4.88	228
190	4.89	316
350	4.85	361
500	4.87	345
600	4.88	275
800	4.85	342
1000	4.89	417
1300	4.86	340
1700	4.85	386
3000	4.87	418
4300	4.89	287
7000	4.88	235
8300	4.94	216

TABLE 31

Measurement of K and Q of Forsterite Samples, Sintered at 1150°C and 1200°C for 5 hours, under Different baking Condition

Frequency	Sample No.	After 90 min. baking at 150°C													
		C_1/1150/5		C_2/1150/5		C_2/1200/5		C_3/1150/5		C_3/1200/5		C_4/1150/5		C_4/1200/5	
		K	Q	K	Q	K	Q	K	Q	K	Q	K	Q	K	Q
70 Kc/s	1	5.0	464	4.5	432	6.0	356	6.3	280	6.6	254	2.9	162	4.2	227
	2	5.3	325	4.7	347	6.2	347	6.2	267	6.7	551	3.5	170	3.8	189
	3	5.2	394	4.6	423	6.1	336	6.2	329	6.5	620	3.3	188	3.2	186
	4	6.9	299	5.4	278	8.1	72	7.9	198	9.0	391	4.6	79	4.9	129
1.1 Mc/s	1	5.0	456	4.5	338	6.0	411	6.3	730	6.6	796	3.0	212	4.1	196
	2	5.1	235	4.7	355	6.1	453	6.2	708	6.7	726	3.4	244	4.2	181
	3	5.2	363	4.7	351	6.0	399	6.3	493	6.5	578	3.3	233	3.6	195
	4	6.8	474	5.3	255	8.2	217	7.6	528	9.2	579	4.5	111	5.0	201
11 Mc/s	1	5.2	163	4.6	189	6.2	227	6.3	396	6.8	246	3.0	209	4.1	175
	2	5.3	39	4.7	335	6.2	248	6.3	299	6.9	204	3.5	219	4.2	197
	3	5.2	108	4.6	338	6.2	185	6.3	493	6.8	188	3.3	204	4.1	226
	4	7.1	462	5.2	373	7.7	314	8.0	470	9.3	549	4.6	141	5.2	295

...Contd.

TABLE 31

Measurement of K and Q of Forsterite Samples, Sintered at 1150°C and 1200°C for 5 hours, under Different baking Condition

Frequency	Sample No.	After 90 min. baking at 150°C													
		C_1/1150/5		C_2/1150/5		C_2/1200/5		C_3/1150/5		C_3/1200/5		C_4/1150/5		C_4/1200/5	
		K	Q	K	Q	K	Q	K	Q	K	Q	K	Q	K	Q
70 Kc/s	1	5.0	464	4.5	432	6.0	356	6.3	280	6.6	254	2.9	162	4.2	227
	2	5.3	325	4.7	347	6.2	347	6.2	267	6.7	551	3.5	170	3.8	189
	3	5.2	394	4.6	423	6.1	336	6.2	329	6.5	620	3.3	188	3.2	186
	4	6.9	299	5.4	278	8.1	72	7.9	198	9.0	391	4.6	79	4.9	129
1.1 Mc/s	1	5.0	456	4.5	338	6.0	411	6.3	730	6.6	796	3.0	212	4.1	196
	2	5.1	235	4.7	355	6.1	453	6.2	708	6.7	726	3.4	244	4.2	181
	3	5.2	363	4.7	351	6.0	399	6.3	493	6.5	578	3.3	233	3.6	193
	4	6.8	474	5.3	255	8.2	217	7.6	528	9.2	579	4.5	111	5.0	201
11 Mc/s	1	5.2	163	4.6	189	6.2	227	6.3	396	6.8	246	3.0	209	4.1	175
	2	5.3	39	4.7	335	6.2	248	6.3	299	6.9	204	3.5	219	4.2	197
	3	5.2	108	4.6	338	6.2	185	6.3	493	6.8	188	3.3	204	4.1	226
	4	7.1	462	5.2	373	7.7	314	8.0	470	9.3	549	4.6	141	5.2	295

...Contd.

Table 31 (...Contd.)

Frequency	Sample No.	After 150 minutes baking at 150°C													
		C_1/1150/5		C_2/1150/5		C_2/1200/5		C_3/1150/5		C_3/1200/5		C_4/1150/5		C_4/1200/5	
		K	Q	K	Q	K	Q	K	Q	K	Q	K	Q	K	Q
70 Kc/s	1	4.9	436	4.3	608	5.8	409	6.4	412	6.4	943	2.7	319	3.8	292
	2	4.9	424	4.1	554	5.6	259	6.4	887	6.4	892	3.2	250	3.6	254
	3	4.9	393	4.0	524	5.8	430	6.4	419	6.2	909	2.9	210	3.7	294
	4	6.0	181	4.4	381	5.9	397	6.8	124	6.7	551	3.7	94	4.2	57
1.1 Mc/s	1	4.8	447	4.3	255	5.8	386	6.3	997	6.4	1048	2.7	273	3.8	188
	2	4.9	381	4.1	405	5.6	727	6.2	484	6.4	1000	3.1	293	3.6	177
	3	4.9	304	4.1	259	5.8	515	6.4	889	6.2	921	2.8	150	3.8	208
	4	4.8	349	4.2	292	6.1	368	7.4	1769	6.6	786	3.5	135	3.4	196
11 Mc/s	1	5.0	134	4.4	60	5.9	234	6.4	437	6.6	254	2.7	218	3.9	132
	2	5.0	110	4.2	338	5.7	271	6.3	66	6.7	254	3.2	245	3.7	162
	3	4.9	68	4.1	91	6.0	193	6.5	460	6.6	189	2.9	139	3.8	210
	4	4.7	537	4.3	181	5.4	685	7.5	1600	6.5	875	3.5	242	3.4	282

TABLE 32

Measurement of K and Q of Electroded Forsterite Samples Using Parallel Plate Set up

Frequency Kc/s	I		V		VII	
	K	Q	K	Q	K	Q
105	5.77	227	6.70	57	5.89	82
2600	5.97	200	6.77	149	5.91	83
11500	5.60	85	6.53	71	5.79	33

TABLE 33

Measurement of K and Q of Electroded Forsterite Samples Using Parallel Plate Setup with Sharp and Flat Contacts at Either Ends

Frequency Kc/s	I		VII		V*	
	K	Q	K	Q	K	Q
105	6.62	424	6.54	175	7.68	33
2600	6.81	262	6.93	200	7.58	69
11500	6.77	91	6.64	56	7.67	157

*For this sample same assembly was used but with wire scratched at a portion.

TABLE 34

Measurement of K and Q of Air by the Unguarded Capacitance Cell

Air gap cm	55 Kc/s		80 Kc/s	
	K	Q	K	Q
0.025	1.28	2832	1.62	889
0.050	1.21	2161	2.02	1752
0.075	1.28	758	2.51	2517
0.100	1.33	985	3.00	709
0.125	1.38	818	3.48	2032
0.150	1.48	625	3.96	339
0.175	1.55	1975	4.43	1849
0.200	1.63	1213	4.91	519
0.250	1.63	2916	5.89	324
0.300	1.82	2720	6.84	989
0.350	1.95	2496	7.78	470
0.400	2.16	1607	8.74	462
0.500	2.26	2019	10.68	452

TABLE 35

Measurement of ΔC and Q of Unguarded Forsterite Samples Using Capacitance Cell.

Frequency Mc/s	Air gap + sample, cm	XIII Without electroding		With electroding		With electroding by thick paint	
		ΔC	Q	ΔC	Q	ΔC	Q
55	0.500	2.2	14	2.4	170	1.9	75
	0.400	4.9	13	4.9	340	4.1	97
	0.350	11.7	16	6.7	240	5.9	140
	0.300	11.9	7	10.2	540	9.7	280
	0.275	16.4	6	13.5	570	12.4	320
	0.250	26.4	4	14.6	310	16.8	390
	0.225	37.1	1	27.4	300	25.6	270

When sample is touched: Without electroding K = 5.70
With electroding K = 4.14
With electroding by thicker paint K = 3.86

TABLE 36

Measurement of ΔC and Q of Unguarded Forsterite Sample with Varying Electrode Baking Time Using Capacitance Cell

Frequency Kc/s	Air gap + sample, cm	XIV Unelectroded		With electroding 20 min. baking		With electroding 120 min. baking	
		ΔC	Q	ΔC	Q	ΔC	Q
	0.500	1.7		1.2	96	1.9	150
	0.400	3.2	160	2.5	120	3.1	180
	0.300	6.2	84	5.2	82	5.8	330
55	0.250	9.4	65	7.9	68	8.2	380
	0.200	15.2	41	13.2	49	13.3	510
	0.175	22.7	30	19.1	36	18.3	700
	0.150	40.4	25	31.0	23	29.9	450
	0.125	Unmeasurable		74.6	11	57.0	230

When sample is touched:

With electroding, 20 min. baking $K = 6.10$
With electroding, 120 min. baking $K = 4.61$

TABLE 37

Measurement of K and Q of Air Using Capacitance Cell

Frequency	Air gap cm	Guard and shield both grounded		Unguarded, shield grounded		Guard ring having same potential and shield grounded		Upper electrode soldered, unguarded, shield grounded		Ungrounded and unshielded	
		K	Q	K	Q	K	Q	K	Q	K	Q
55 Kc/s	0.500	6.27	16	7.09	25	6.58	26	6.04	29	1.29	178
	0.200	4.87	17	5.33	24						
	0.100	3.55	24	3.47	35	3.65	40	2.79	25		
	0.070	3.13	32	2.85	35						
	0.050	2.79	45	2.36	41						
	0.025	2.80	90	1.71	47	2.69	112	1.35	47	0.36	285
100 Kc/s	0.300	6.66	14	8.47	45						
	0.200	5.19	16	5.70	45						
	0.100	3.71	25	3.67	50						

. . Contd.

Table 37 (...Contd.)

Frequency	Air gap cm	Guard and shield both grounded		Unguarded, shield grounded		Guard ring having same potential and shield grounded		Upper electrode soldered, unguarded, shield grounded		Ungrounded and unshielded	
		K	Q	K	Q	K	Q	K	Q	K	Q
	0.300	6.03	35	6.97	65	11.47	42	5.71	42	1.81	114
	0.200	4.81	41	5.29	75						
	0.100	3.50	58	3.44	76	3.54	65	2.7[illegible]	40		
1 Mc/s	0.070			2.85	70						
	0.050	2.73	91	2.55	54						
	0.025	2.45	162	1.67	98	2.68	239	1.54	100	0.36	210
	0.300	6.28	49								
	0.200	5.06	55								
10 Mc/s	0.100	3.76	68								
	0.050	3.09	85								

TABLE 38

Measurement of ΔC and Q of Air Using Capacitance Cell

Air gap	1 Mc/s			55 Kc/s		
cm	A/t cm	ΔC	Q	A/t cm	ΔC	Q
0.500	39.30	30.3	48	39.30	30.7	33
0.400	49.12	32.2	42	49.12	32.8	35
0.300	65.49	35.2	49	45.49	35.5	38
0.200	98.24	41.3	62	98.24	41.7	38
0.100	196.49	58.0	77	196.49	58.5	49
0.050	392.97	87.3	124	392.97	86.2	73
0.025	785.94	135.7	201	785.94	135.1	114

TABLE 39

Measurement of ΔC and Q of Air Using Capacitance Cell

Frequency	Air gap cm.	Unshielded, unguarded Arrangement 1 C	Q	Arrangement 2 C	Q	Shield earthed, unguarded Arrangement 1 C	Q	Arrangement 2 C	Q
70 Kc/s	0.025	45.2	537	43.6	602	72.2	406	79.7	439
	0.100	14.8	202	15.3	254	27.5	169	29.0	164
	0.300	8.4	114	9.0	206	16.3	124	17.2	97
	0.500	7.8	109	8.0	114	13.3	122	14.9	87
1Mc/s	0.025	47.9	611	43.1	440	71.1	334	78.4	379
	0.100	15.1	120	15.4	157	26.6	125	28.7	139
	0.300	8.5	73	9.4	109	16.9	191	17.0	87
	0.500	6.6	75	7.9	91	14.6	377	15.3	54

Arrangement 1 ; Using pin connector

Arrangement 2 ; Pin connector was not used.

TABLE 40

Measurement of K and Q of Unelectroded and Unguarded Sample (XVII) Along with Air Using Capacitance Cell

Frequency	Air gap + Sample cm	Unshielded Arrangement 1 K	Unshielded Arrangement 1 Q	Shield earthed Arrangement 2A K	Shield earthed Arrangement 2A Q	Shield earthed Arrangement 2B K	Shield earthed Arrangement 2B Q	Shield earthed Arrangement 1 K	Shield earthed Arrangement 1 Q
55 Kc/s	0.500			--	1548				
	0.300			--	760				
	0.200			--	1187				
	0.111*			5.49	137				
70 Kc/s	0.500	--	2402					--	678
	0.300	--	801					--	2133
	0.200	--	--					--	--
	0.111*	3.8	488					5.84	727
90 Kc/s	0.500					--	1353		
	0.300					--	2309		
	0.111*					6.65	654		

...Contd.

Table 40 (...Contd.)

Frequency	Air gap + sample cm	Unshielded Arrangement 1 K	Unshielded Arrangement 1 Q	Shield earthed Arrangement 2A K	Shield earthed Arrangement 2A Q	Shield earthed Arrangement 2B K	Shield earthed Arrangement 2B Q	Shield earthed Arrangement 1 K	Shield earthed Arrangement 1 Q
1 Mc/s	0.500			--	1473			--	3138
	0.300			--	6134			--	7713
	0.200			--	3357			--	--
	0.111*			5.66	1007			5.99	1609
1.5 Mc/s	0.500	-	3504			--	2220		
	0.300	-	974			--	4727		
	0.111*	5.2	820			6.52	1241		

*Sample was touched at this thickness by two electrodes, in other stages measurement was taken using air and sample.

Arrangement 1: Pin connector was used

Arrangement 2A: Pin connector was not used.

Arrangement 2B: Pin connector was not used and $\triangle C:C_1$ was made higher than 2A.

TABLE 41

Measurement of K and Q of Forsterite Samples, Fired at 1200°C for 5 hours, in Capacitance Cell made of Aluminium

Frequency	Batch No.	Sample No.	Guarded, shield ungrounded K	Guarded, shield ungrounded Q	Guarded, shield ground K	Guarded, shield ground Q	Guarded, shield with micrometer cap grounded K	Guarded, shield with micrometer cap grounded Q	Guarded, shield with micrometer cap ungrounded K	Guarded, shield with micrometer cap ungrounded Q
70 Kc/s	C_3	1	9.92	312	11.02	323	11.07	336	10.57	364
		2	10.46	322	10.26	540	11.42	296	10.97	353
		4	22.46	205	25.79	159	24.10	130	23.47	186
	B_3	1	6.70	214	9.97	110	10.84	88	9.52	91
		2	8.18	186	12.52	131	12.56	113	10.27	84
		3	8.57	234	10.10	120	9.56	100	9.58	90
		4	19.17	54	20.97	24	22.32	24	21.23	15
1.1 Mc/s	C_3	1	9.92	504	10.99	506	11.05	503	10.40	584
		2	10.49	486	10.45	481	11.16	453	10.94	513
		4	22.46	239	24.80	192	28.00	215	25.55	262
	B_3	1	6.72	361	9.88	269	10.64	240	9.12	272
		2	7.82	411	12.52	294	12.69	164	10.18	238
		3	8.72	453	10.67	319	9.55	232	9.54	263
		4	19.24	152	21.68	111	24.38	86	20.84	62
11 Mc/s	C_3	1	11.82	106	Unmeasurable C_2		Unmeasurable C_2		12.50	258
		2	12.24	260	14.70	76	16.05	69	12.87	253
		4	22.85	241	28.25	127	34.31	115	24.10	270
	B_3	1	7.24	293	9.29	81	14.25	81	10.20	276
		2	8.41	314	12.65	79	16.94	77	11.30	254
		3	10.20	256	15.68	59	13.58	67	10.93	232
		4	19.11	199	25.02	112	28.76	92	20.33	148

TABLE 42

Variation of the K Value with Change in Density

Batch No.	Density gms/cc	K 70 Kc/S	1.1 Mc/S	11 Mc/S
C_2	2.05	4.1	4.2	4.2
	2.73	5.7	5.7	5.9
C_3	2.87	6.3	6.3	6.6
	2.88	6.4	6.3	6.4
C_4	1.36	2.9	2.9	2.9
	1.98	3.7	3.7	3.8

TABLE 43

Measurement of K and Q of Electroded and Wired Forsterite Samples

Batch No.	Sample No.	100 Kc/S K	100 Kc/S Q	500 Kc/S K	500 Kc/S Q	1 Mc/S K	1 Mc/S Q	5 Mc/S K	5 Mc/S Q	10 Mc/S K	10 Mc/S Q	25 Mc/S K	25 Mc/S Q	Average Q	Average $\tan\delta \times 10^4$
C_3	1	6.26	388	6.21	615	6.42	535	6.20	608	6.21	625	6.47	924	616	16
	2	6.86	3938	6.48	1071	7.02	1929	6.86	1267	7.24	942	6.75	583	2074	5
	3	5.36	5477	6.37	1355	6.91	3055	6.07	1285	6.71	2419	6.98	1570		
	4	5.92	1285	5.82	682	6.23	1215	6.02	1180	6.13	1625	6.23	1657	1311	8
	5	6.60	900	6.91	1190	7.48	1635	6.81	694	6.46	2410	6.81	1265		
	6	5.08	3424	5.80	624	5.90	615	5.80	667	5.51	1205	6.90	734	1228	8
	7	6.65	752	6.35	2310	6.40	1269	6.55	1304	6.80	1399	5.85			
Pure	PM1	5.30	208	5.36	269	5.36	448	5.30	1480	5.25	1176	5.25	1122	707	14
	PM2	5.85	394	5.80	595	6.02	954	5.57	532	5.57	997	6.02	303		

TABLE 44

Measurement of K of Electroded and Wired Forsterite Samples with Varying Thickness

Batch No.	Sample No.	K					
		100 Kc/S	500 Kc/S	1 Mc/s	5 Mc/S	10 Mc/S	25 Mc/S
	2A	6.86	6.48	7.02	6.86	7.24	6.75
C_3	2B	6.29	6.41	6.25	6.18	6.22	6.37
	2C	6.23	6.30	6.20	6.18	6.19	6.28

Sample thickness: 2A - 0.5464 cm

2B - 0.3804 cm

2C - 0.2520 cm

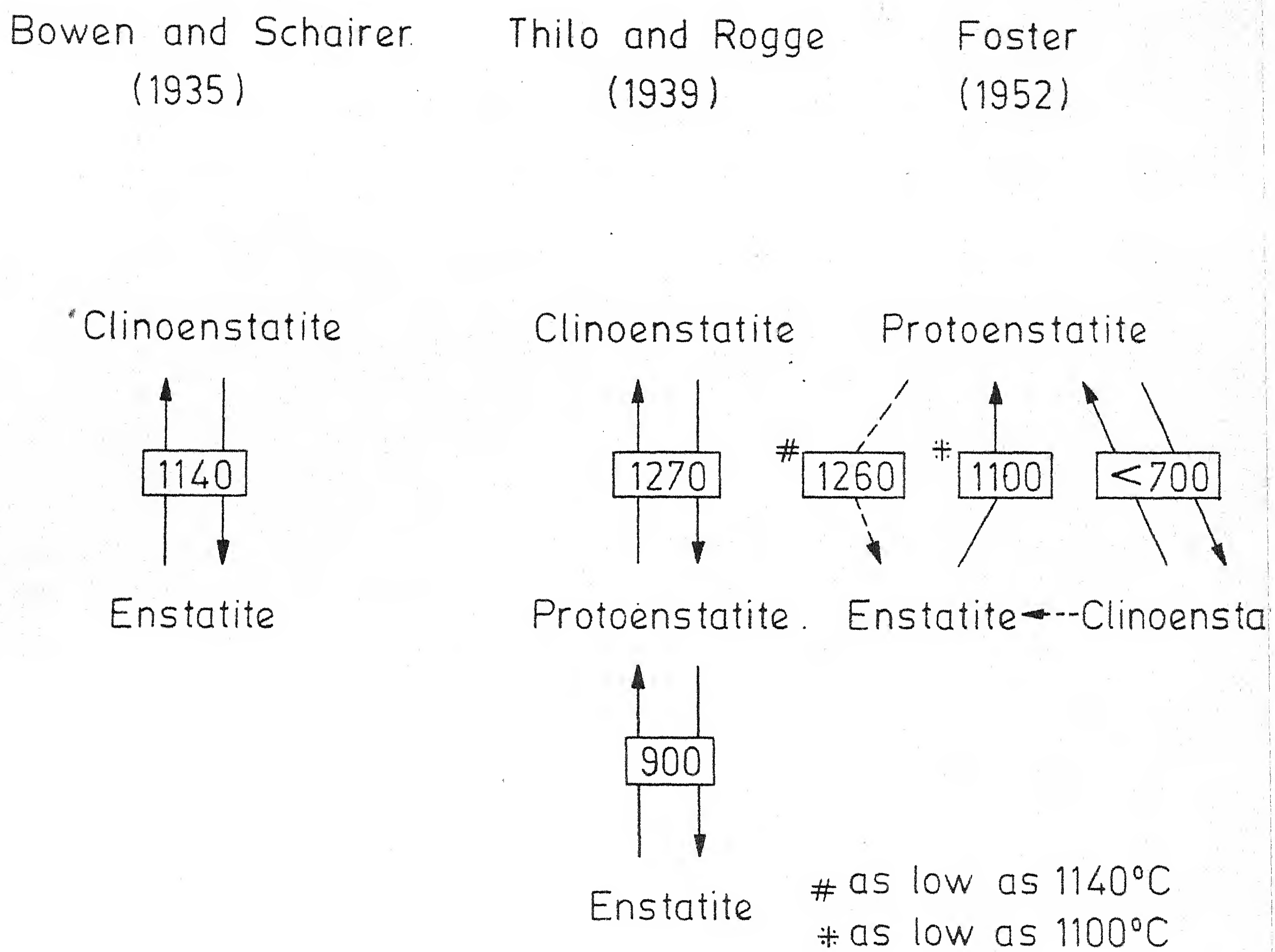

Fig. 1 Schemes of polymorphism of $MgSiO_3$.
(Ref. 5)

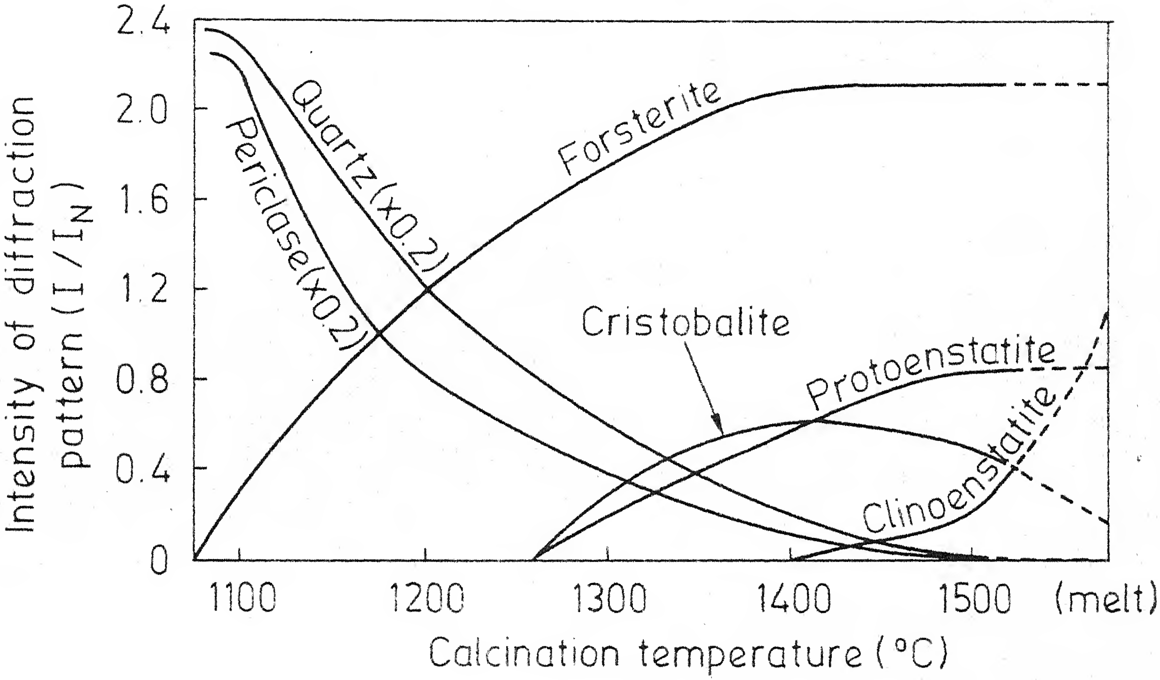

Fig 2 Intensity of diffraction patterns at various temperatures of calcination. (Ref. 6, fig. 1)

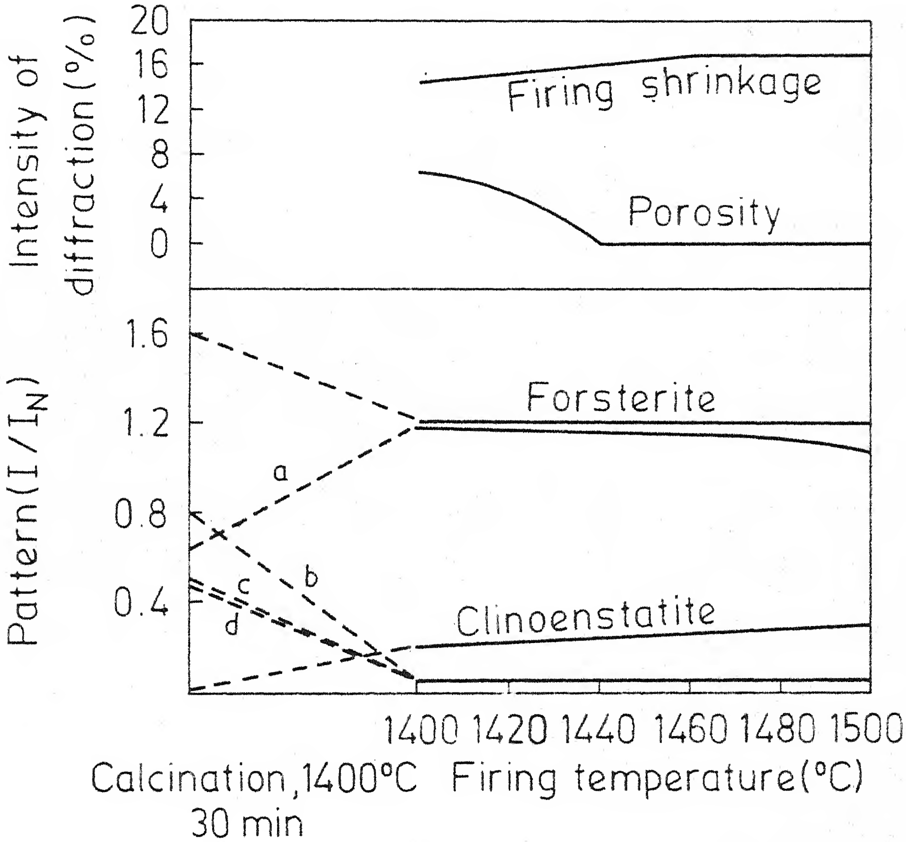

Fig 3 Intensity changes of diffraction pattern of composition 95 % (2 MgO) (1.2 SiO_2) with 5 % Kaolin (PSF - 0) [Ref. 6, fig 3].

(a) Protoenstatite (b) Cristobalite

(c) Quartz (d) Periclase

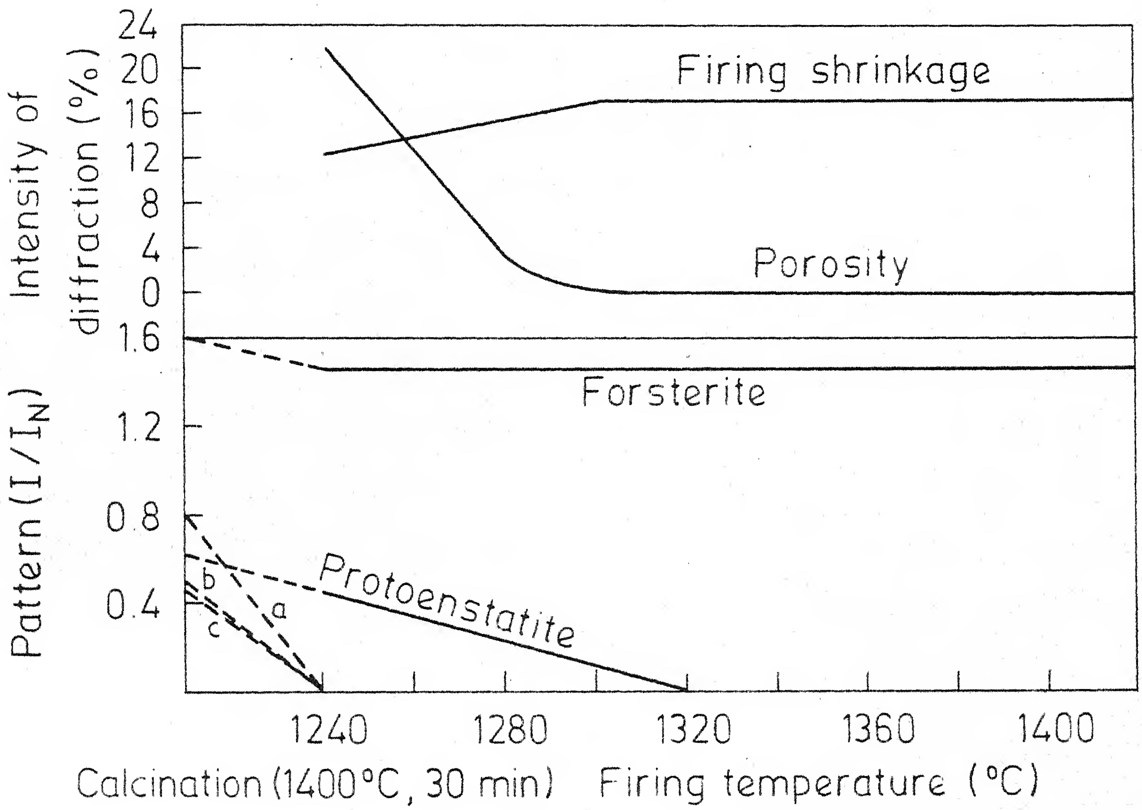

Fig. 4 Intensity changes of diffraction pattern of composition 85 % (2 MgO) (1.2 SiO_2) with 5 % Kaolin and 10 % $BaCO_3$ (PSF - B) [Ref 6, fig. 4].

(a) Cristobalite (b) Quartz (c) Periclase

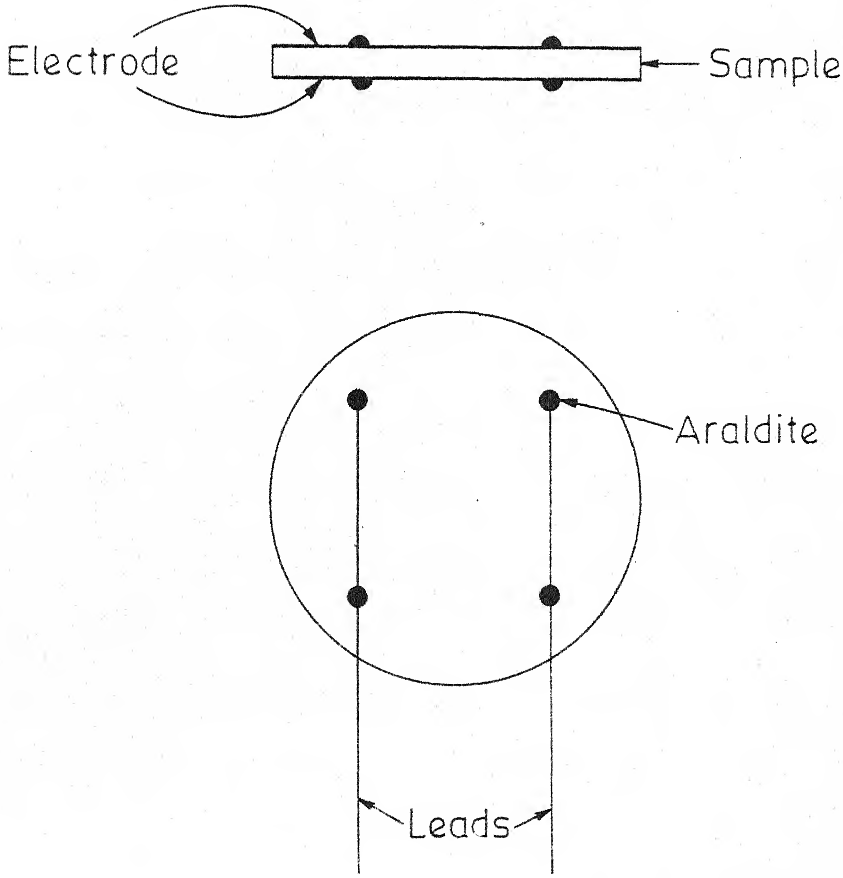

Electroded and wired sample.

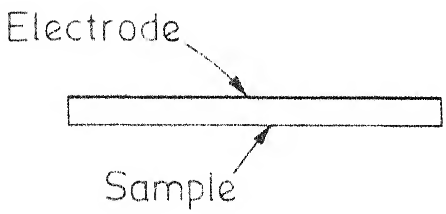

One side electroded sample

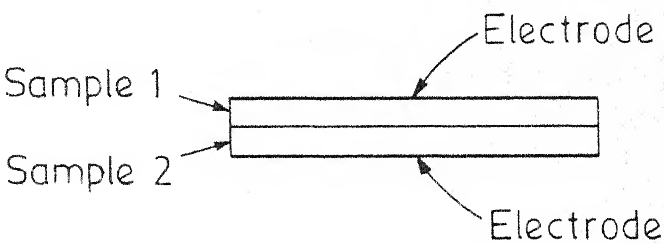

Sandwitch of two one side electroded sample

Fig. 6 Sketch of electroded and wired forsterite samples.

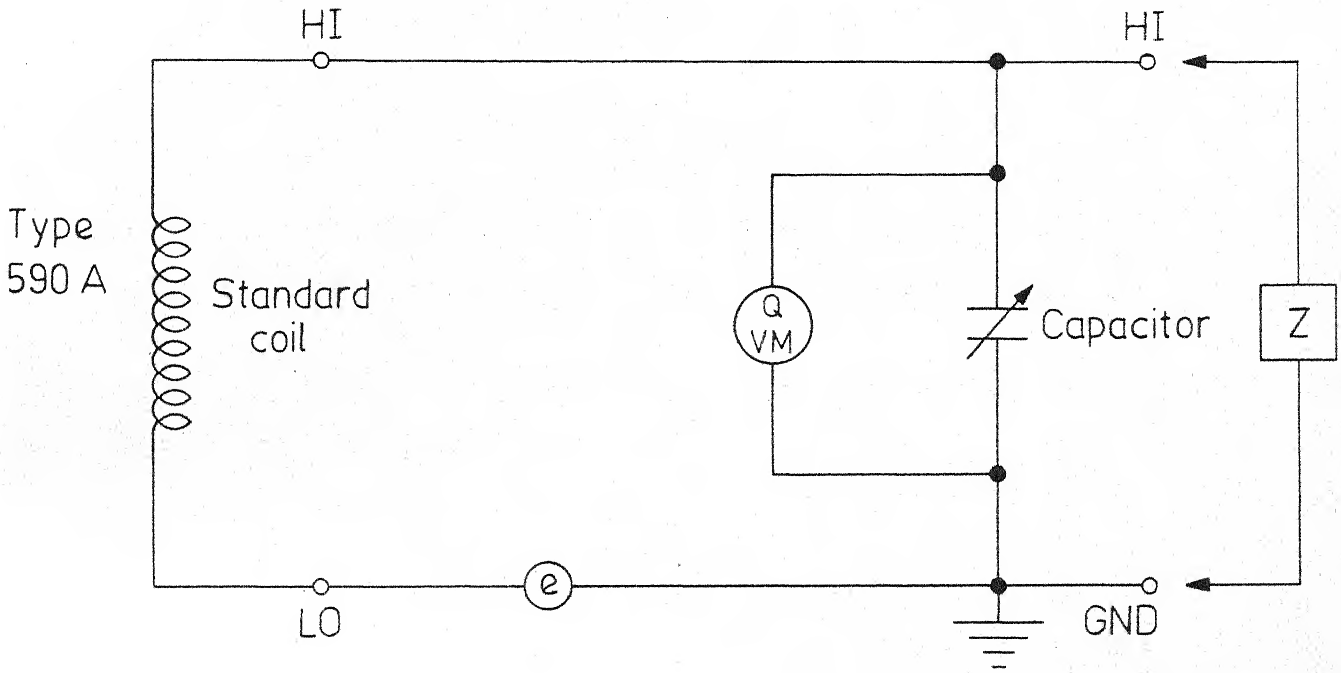

Fig. 7 Circuit for measuring the dielectric constant and Q-factor of the sintered disc samples by parallel connection. (details in appendix I)

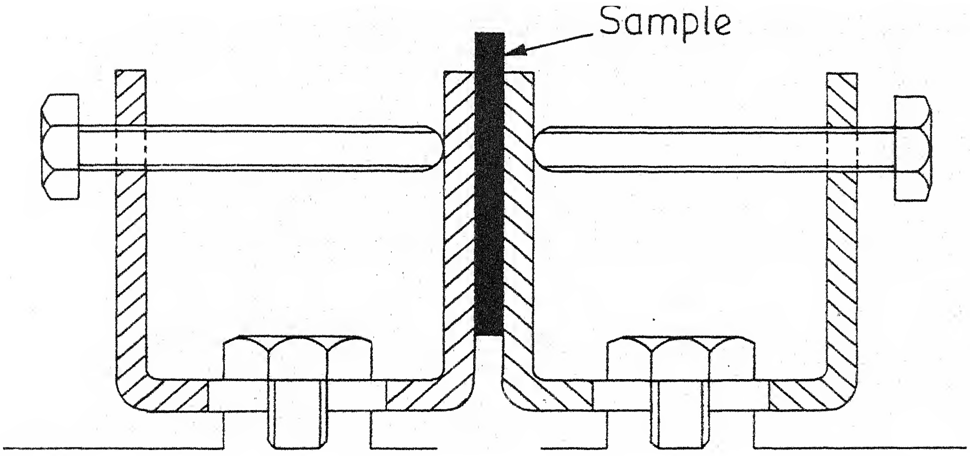

Elevation (arragement 1)

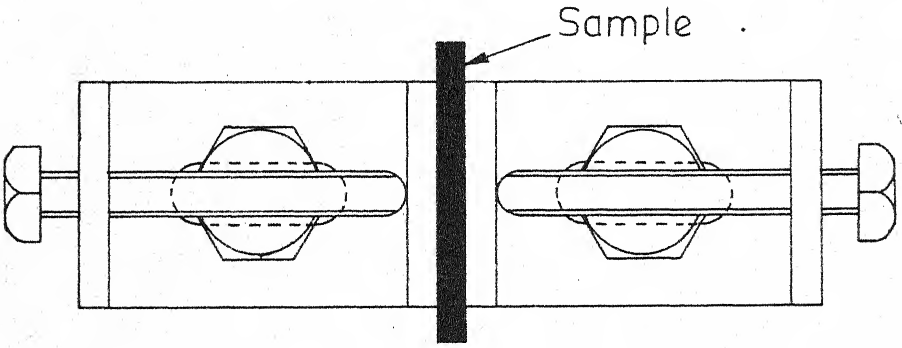

Plan (arrangement 1)

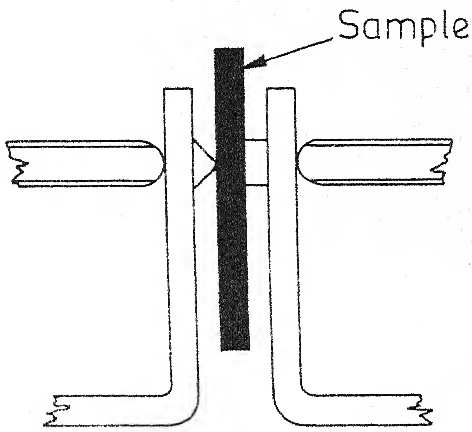

Elevation (arrangement 2)

Fig. 8 Sketch of parallel plate setup for measuring K, the dielectric constant and Q, the quality factor of sintered forsterite sample.

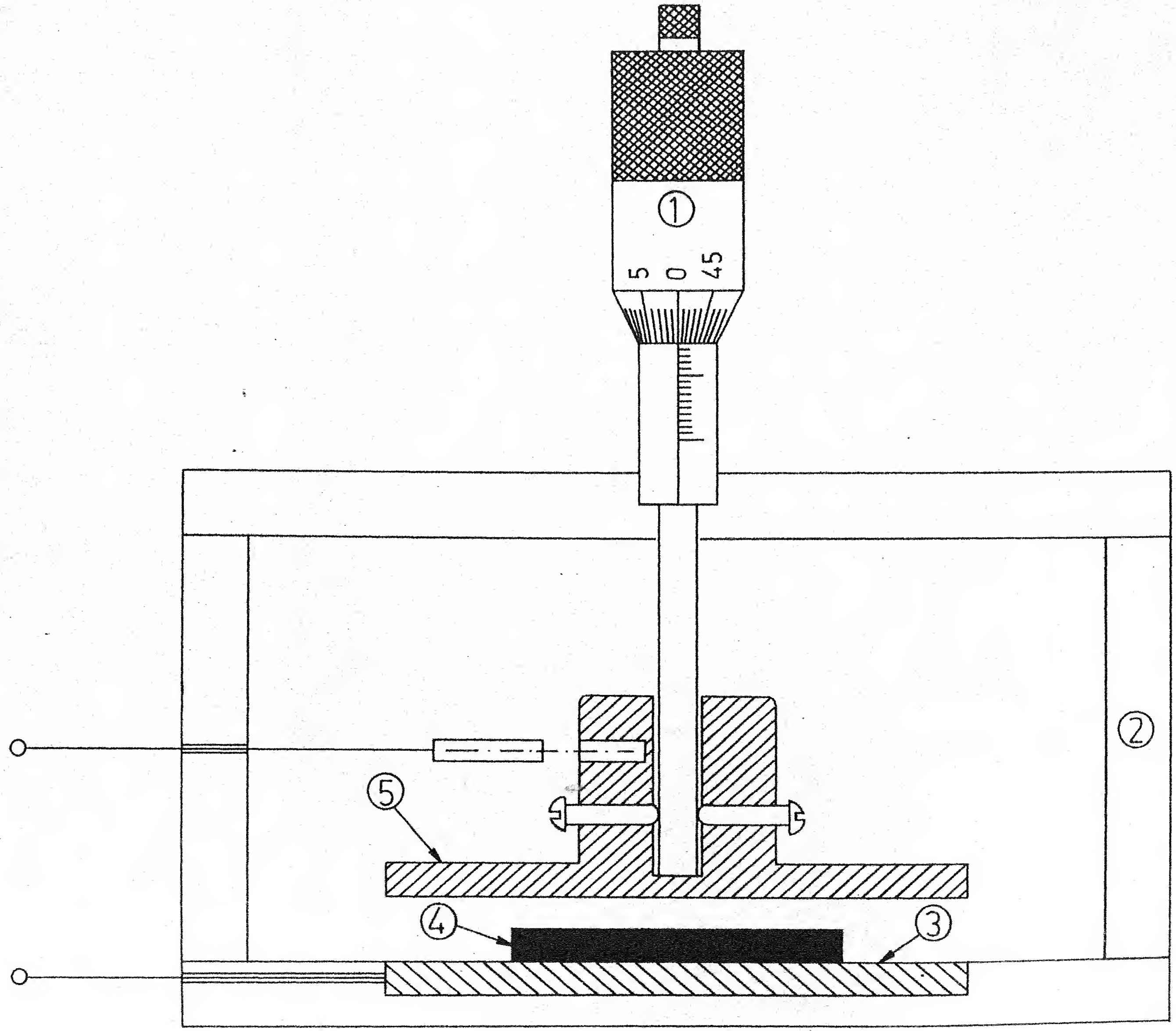

Fig 9 Sketch of unguarded and unshielded capacitance cell for measuring K, the

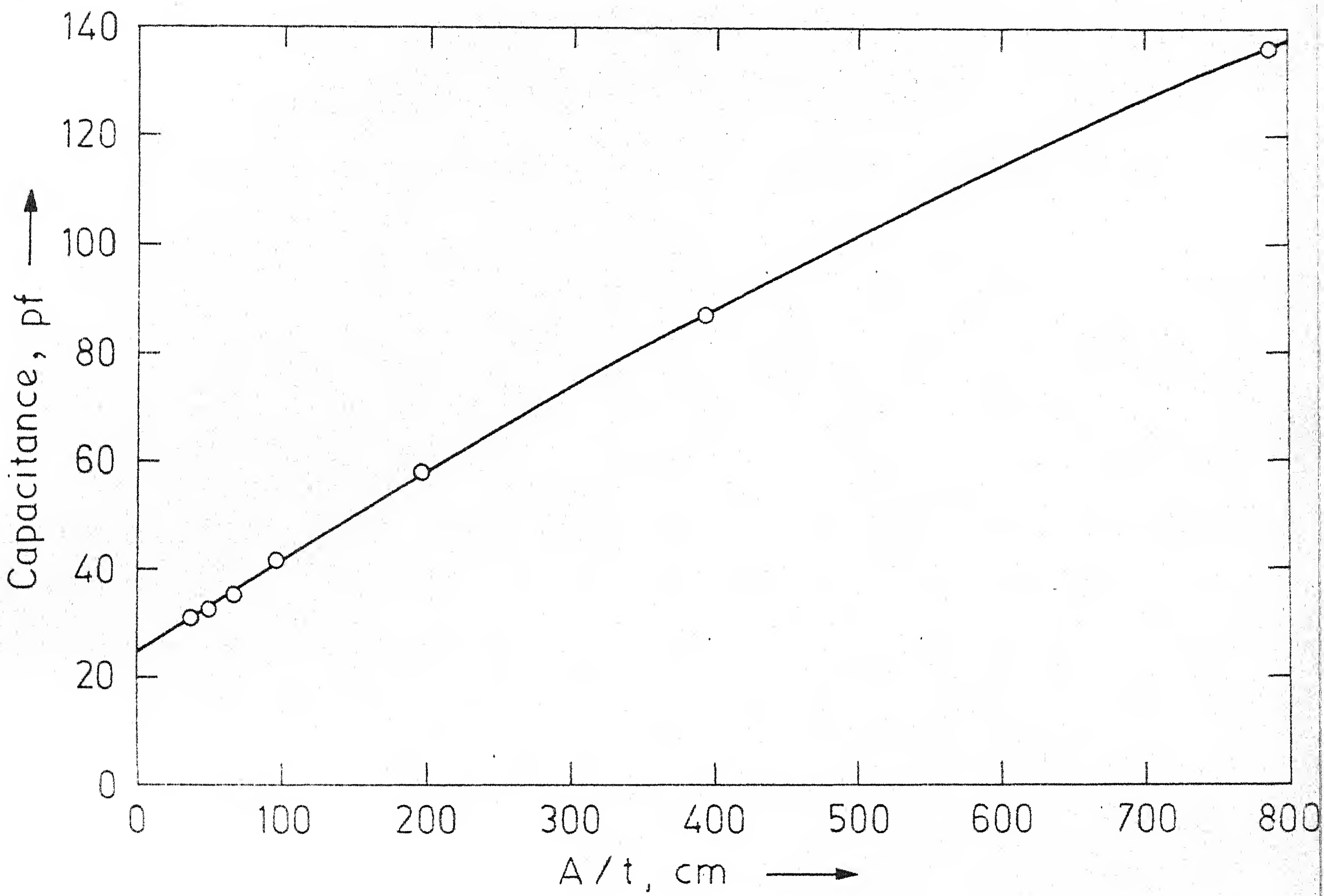

Fig. 11 C versus A / t plot for finding out actual K value of air.

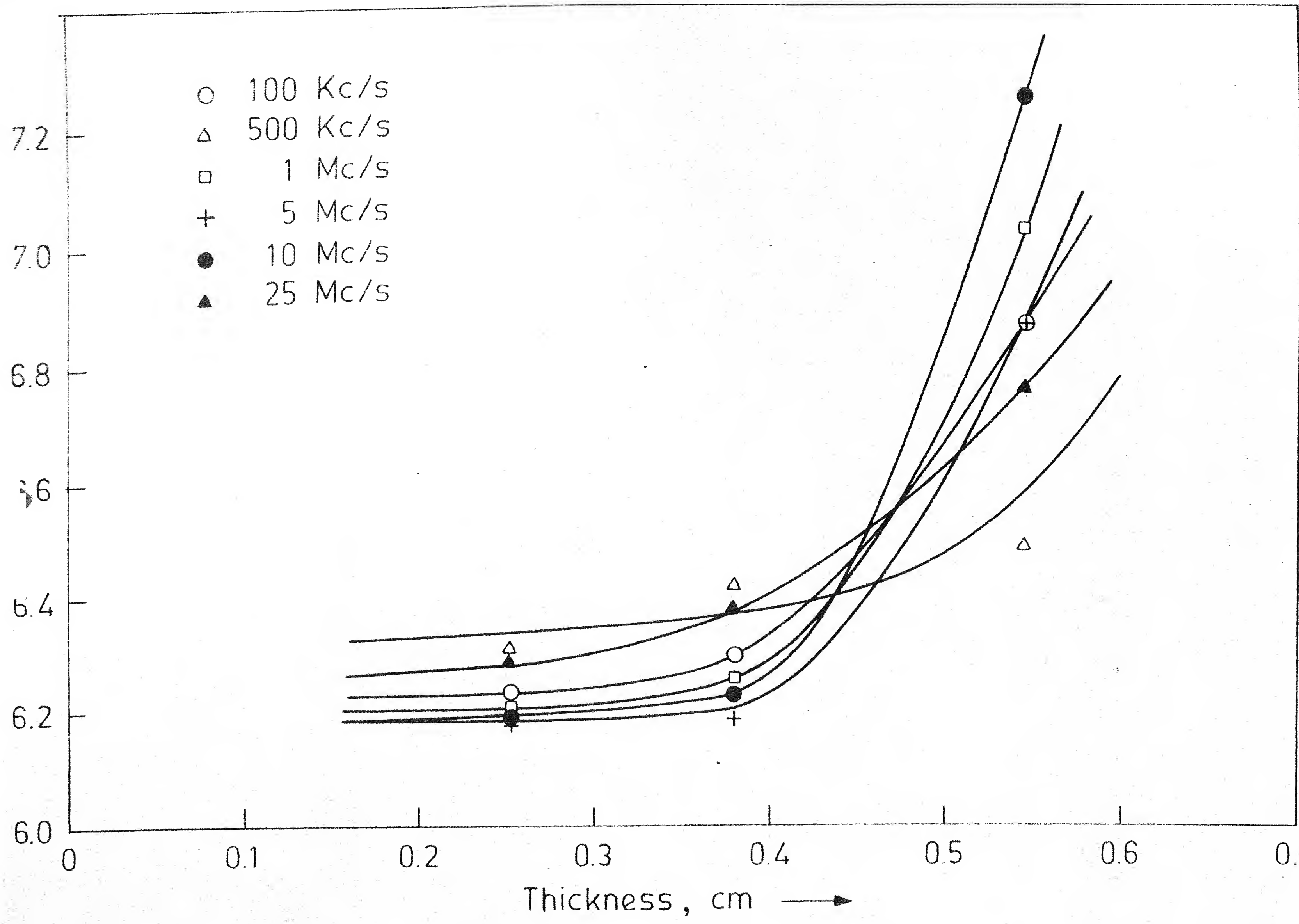

Fig. 12 Variation of relative dielectric constant K with sample thickness for a forsterite

REFERENCES

1. L. Navais, 'Advances in Ceramics Related to Electronic Tube Developments', Jr. Am. Cer. Soc. 37(8), 329-350 (1954).

2. L. Atlas, 'The Polymorphism of $MgSiO_3$ and Solid-State Equilibria in the System $MgSiO_3$-$CaMgSi_2O_6$', Jr. Geology 60(2), 125-47 (1952).

3. Hans Thurnauer, 'Low-loss Ceramic Dielectric', Tele. Tech., 6 (2), 86-87, 130 (1947).

4. V. D. Zaikina, 'Formation of Clinoenstatite in Synthetic Forsterite', (Met. Inst. Dneprepetrovsk) Ogneupouf 20(2), 79-82 (1955); Chem. Abstr. 50 (1956) 8153h.

5. W. R. Foster, 'High Temperature X-ray Diffraction Study of the Polymorphism of $MgSiO_3$', Jr. Am. Cer. Soc. 34(9), 255-59 (1951).

6. M. Sugiura, M. Hirai, E. Ishii and S. Sano, 'Forsterite Porcelain as High Frequency Insulator, I : 'Properties of Forsterite Containing Excess Silica', Jr. Ceram. Assoc. Japan 67(10), 333-344 (1959).

7. R. Hayami and T. Ogura, 'Kinetics and Mechanism of Formation of Forsterite by Solid State Reaction of MgO and Enstatite', Jr. Ceram. Assoc. Japan 75(7), 215-220 (1967).

8. R. Hayami, 'Kinetics and Mechanisms of Formation of Enstatite by Solid State Reaction of Forsterite and SiO_2', Jr. Ceram. Assoc. Japan 75(11), 343-347 (1967).

9. M. Sugiura, M. Hirai, S. Sano and E. Ishii, 'Forsterite Porcelain as a High Frequency Insulator, V: The Relation Between the Microstructure and the Electrical and Mechanical Properties of Forsterite Porcelain', Jr. Ceram. Assoc. Japan 70(6), 181-190 (1962).

10. S. Sano, E. Ishii, M. Hirai and M. Sugiura, 'The Forsterite Porcelain as a High Frequency Insulator, VII: Effect of Kaolin Addition on Properties of Forsterite Porcelain', Jr. Ceram. Assoc. Japan 71(12), 231-236 (1963).

11. M. Sugiura, S. Sano, E. Ishii and M. Hirai, 'Forsterite Porcelain as High Frequency Insulator, IV: The Relation Between the Microstructure and the Thermal Expansion of Forsterite Porcelain', Jr. Ceram. Assoc. Japan 70(4) 100-110 (1962).

12. E. Singer and Chr. Adolf, 'Forsterite Ceramics with the Same Thermal Expansion as Titanium', Ber. Deut. Keram. Ges. 37,3-6 (1960), Chem. Abstr. 54 (1960) 15880e.

13. Compagnie Generale de Telegraphic, 'Ceramics for Low Dielectric Loss', Fans Fil Fr. 1,071,896, Sept. 6 (1954). Chem. Abstr. 55 (1959), 5623a.

14. General Electric Co. Brit. 'Forsterite Ceramic Bodies', 798, 450, July 25 (1958), Chem. Abstr. 53 (1959) 1665e.

15. N. Soga and O. L. Anderson, 'High Temperature Elasticity and Expansivity of Forsterite and Steatite', Jr. Am. Cer. Soc. 50(5) 239-42 (1967), Chem. Abstr. 67 (1967) 46718b.

16. E. Kanchin and V. Amburz, 'Thermal Dilatation of the Minerals in the System CaO-MgO-SiO_2', Chem. Zvesti 19(1), 51-54(1965), Chem. Abstr. 62 (1965), 8701e.

17. E. T. Smoke, 'Inorganic Dielectric Research', Rutgers State Univ. Coll. Res. Bull. 1970 No. 50,531 pp. Chem. Abstr. 72 (1970) 115646u.

18. P. G. Usov et al.(USSR), 'Tremolite, a Raw Material for High Frequency Ceramics', Sb. Tr. Molodykh Uch., Tomsk Polytech. Inst. 1973, No. 1, 87-90 (Russ), Chem. Abstr. (1974).

19. P. G. Usov et al. (USSR), 'Kinetics of Sintering of Forsterite Ceramics Produced from Magnesium Oxide Obtained by Various Methods', ibid. (1973), No. 1, 86-87 (Russ), Chem. Abstr.(1974).

20. P. G. Usov et al. (USSR), 'Preparation of Vacuum Compact High Frequency Dielectrics from Alguisk Talc', ibid. (1973), No. 1, 101-103(Russ), Chem. Abstr.(1974).

21. S. K. Gupta and A. R. Das, 'Effect of Processing Parameters on Microstructure Development and Magnetic Spectrum of $Ni_{0.3}Zn_{0.7}Fe_2O_4$ Ferrite: II - Magnetic Spectrum and its Correlation with Sintering Conditions and Microstructure', Tr. Ind. Cer. Soc. XXXVI (3), 55-60 (1977).

22. A. R. Das, 'Forsterite Ceramics for Low Loss Applications', Report No. CSIR-MT-(ARD)/77-79/29/I, December 1977, IIT Kanpur.

23. P. K. Ghosh and A. R. Das, 'Forsterite Ceramics for Low Loss Applications: Literature Review, X-ray Analysis, Sample Fabrication and Investigation of Experimental Errors, Report No. CSIR-MT-(ARD)/77-79/29/II, October 1978.

24. A. R. von Hippel, Editor, 'Dielectric Materials and Applications', Technology Press, Cambridge, Massachusetts, John Wiley and Sons., New York, 1954.

25. L. Bragg and G. F. Claringbull, 'Crystal Structures of Minerals', Chap. IX p. 73, G. Bel,London (1965).

26. R. W. G. Wycoff, 'Crystal Structures', Vol. III, Chap.XII, aI 4, Interscience, New York.

27. W. D. Kingery, H. K. Bowen, D. R. Uhlmann, 'Introduction to Ceramics', Chap. 18, p. 947, John Wiley and Sons (1975).

28. 1967 Book of ASTM Standards, 'Electrical Insulating Materials', Part 29, p. 86, American Society for Testing and Materials.

APPENDIX - I

Q-meter is an exceedingly useful instrument for measuring the characteristics of coils and capacitors at radio frequencies. The ratio between the voltage developed across the capacitive portion (C) of the resonant test circuit and the voltage injected into the circuit is actually measured.

$Q = \frac{X}{R} = \frac{V_c}{e}$, where e is the voltage injected into the test circuit and V_c is the voltage measured across the capacitor at resonance. e is maintained at 0.01 volt; therefore 100 V_c will be equal to the circuit Q and the meter can be calibrated to read Q directly. This has been done in the 260-AP. In the equation above, X is the reactance of either the capacitor or the inductor, the values being equal at resonance; R is the sum of the resistances of the unknown and of the internal circuit, and the resultant Q reading is that of the circuit, rather than that of the unknown component alone. In most cases the Q of the unknown and the Q of the circuit differ by a negligible amount.

Derivation of the formulae used in Q-meter measurements are given below.

If the circuit is resonated at a value C_1, with a Q-reading of Q_1 before introducing the unknown, then

$$\frac{1}{\omega C_1} = \omega L \qquad (1)$$

where L = Inductance

ω = $2\pi f$, where f = Frequency

C_1 = Capacitance

and

$$Q_1 = \frac{\omega L}{R} = \frac{1}{\omega C_1 R} \qquad (2)$$

where R = Resistance.

The characteristics of an unknown connected in parallel are expressed most simply in terms of parallel X_p (Inductive or Capacitive reactance) and R_p. After the preliminary balance the addition of X_p requires a decrease in tuning capacitance (if X is capacitive) to a new value C_2 and (C_2-C_1) is the effective parallel capacitance of the unknown. Now,

$$X_p = \frac{1}{\omega(C_2 - C_1)} \qquad (3)$$

and

$$\frac{1}{R_p} = \frac{\omega C_1}{Q_2} - \frac{R}{R^2 + \omega^2 L^2}$$

$$\doteq \frac{\omega C_1}{Q_2} - \frac{1}{R} \cdot \frac{1}{1 + \frac{\omega^2 L^2}{R^2}}$$

$$= \frac{\omega C_1}{Q_2} - \frac{1}{R Q_1^2}$$

(Replacing $1 + Q_1^2$ by Q_1^2, since $Q_1 \gg 1$).

Using $Q_1 = \frac{1}{\omega C_1 R}$, we get $R_p = \frac{Q_1 Q_2}{\omega C_1 (Q_1 - Q_2)}$ (4)

Therefore, $Q_x = \frac{R_p}{X_p} = \frac{(C_2 - C_1)\, Q_1 Q_2}{C_1 \,(Q_1 - Q_2)}$. (5)

APPENDIX - II

A dielectric material reacts to an electric field differently from a free space because it contains charge carriers that can be displaced, and charge displacements within the dielectric can neutralise a part of the applied field. Since, $V = Q/C$, where V is the applied voltage and Q is the electrical charge that can be stored, and $C = K' C_o$, where K' is relative dielectric constant and C_o is the capacitance in vacuum, we can write for a capacitor containing a dielectric

$$V = \frac{Q/K'}{C_o} \qquad (1)$$

That is, only a fraction of the total charge, the free charge Q/K', sets up an electric field and voltage toward outside; the remainder, the bound charge, is neutralised by polarization of the dielectric. The total electric flux density D can be represented as the sum of the electric field E and dipole charge P:

$$D = \varepsilon_o E + P = \varepsilon' E \qquad (2)$$

where the polarization is the surface charge density of the bound charge, equal to dipole moment per unit volume of material. In the above equation, ε_o and ε' are the dielectric permittivity of vacuum and the dielectric material respectively.

In an ideal capacitor the electric charge adjusts itself instantaneously to any change in voltage. In practice, however, there is an inertia to charge movement that shows up as a relaxation time for charge transport and we have a dependence of dielectric constant on frequency. If the applied electric field is alternating at sufficiently low frequencies the polarization will also alternate. With increasing frequency, the polarization will eventually have difficulty in following the field and will not have time to attain its full value before the field reverses. With increasing frequency in this range the relative permittivity decreases (the 'dispersion' of the relative permittivity) and there is also a loss, or absorption, of electrical energy which causes heating in the dielectric. The electronic polarization is the only process sufficiently rapid to follow alternative fields in the visible part of the spectrum. Ionic polarization processes are able to follow an applied high frequency field and contribute to the dielectric constant at frequencies up to the infrared region of the spectrum. Orientation and space polarization have relaxation times corresponding to the particular system and process but, in general, participate only at lower frequencies.

In discussing the properties of a dielectric, it is convenient to imagine the material situated between the electrodes of a capacitor. However, similar considerations

apply wherever the material appears in an electric field, e.g. as insulation on wires forming connecting leads or coils, or in the electric field associated with electromagnetic wave propagation.

Considering a perfect loss free capacitor (e.g. two plane parallel plates in a vacuum) of capacitance C, having an applied alternating electric potential defined by the equation:

$$E = E_o \cos \omega t \tag{3}$$

where E is the potential at time t, E_o is the maximum value of the potential, ω is the frequency in radians per second, and t is the time.

The displacement current vector is 90 degrees out of phase with the potential. Thus, there is zero component of the current in phase with the potential and no electrical energy is lost by conversion to heat.

If a dielectric is placed in the capacitor the displacement current vector will be slightly less (δ) than 90 degrees ahead of potential. Representing the electric field and displacement (flux density) in complex notation:

$$E = E_o e^{i\omega t} \tag{4}$$

$$D = D_o e^{i(\omega t - \delta)} \tag{5}$$

and making use of the relation

$$D = K^* E \tag{6}$$

one obtains

$$K^{*} = K_s \, e^{-i\delta} = K_s \, (Cos\delta - i \, Sin\delta) \qquad (7)$$

where $K_s = D_o/E_o$ is the static dielectric constant. In terms of a complex dielectric constant,

$$K^{*} = K' - iK'' = \frac{\varepsilon^{*}}{\varepsilon_o} = \frac{1}{\varepsilon_o} (\varepsilon' - i\varepsilon'') \qquad (8)$$

one has from Eq. 7

$$K' = K_s \, Cos\delta \qquad (9)$$

$$K'' = K_s \, Sin\delta \qquad (10)$$

and from Eqs. 9 and 10 the loss tangent is given by,

$$\tan \delta = K''/K' = \varepsilon''/\varepsilon' \qquad (11)$$

This phase shift corresponding to a time lag between an applied voltage and induced current causes loss currents and energy dissipation in ac circuits which do not require charge carrier migration.

The maximum dielectric loss occurs when the period of the relaxation process, whatever it may be, is the same as the period of the applied field. When the relaxation time is large compared with the period of the applied field, losses are small. Similarly when the relaxation process is rapid compared with the frequency of the applied field, losses are small.

The frequency dependence of the relative permittivity ε' and dielectric loss factor ε'' for relaxation absorption are

described by the 'Debye' equations.

$$\varepsilon' = \varepsilon'_{\alpha} + \frac{\varepsilon'_{0} - \varepsilon'_{\alpha}}{1+\omega^{2}\tau^{2}} \qquad (12)$$

$$\varepsilon'' = (\varepsilon'_{0} - \varepsilon'_{\alpha})\frac{\omega\tau}{1+\omega^{2}\tau^{2}} \qquad (13)$$

$$\therefore \tan\delta = \frac{\varepsilon''}{\varepsilon'} = \frac{(\varepsilon'_{0} - \varepsilon'_{\alpha})\omega\tau}{\varepsilon'_{0} + \varepsilon'_{\alpha}\omega^{2}\tau^{2}} \qquad (14)$$

where ε'_0 and ε'_α are the relative permittivities below and above the absorption respectively; the factor $\varepsilon'_0 - \varepsilon'_\alpha$ being termed the dissipation of the relative permittivity;   is the frequency in radians per second; and τ is the relaxation time of the system, which characterizes the rate of build up or decay of the polarization when an electric field is suddenly applied or removed.

The above equations apply to both liquids and solids although different models are used in their derivation.

The Debye equations are based on the assumption that the transient polarization can be represented by a simple exponential with a single relaxation time. Hence any model which predicts a simple exponential rise of polarization on applying a field will, in an ac field, lead to dielectric dispersion and absorption curves of the form given by eqns. 12, 13 and 14. For most materials, however, the experimental values are not well described by the Debye equations.

Energy losses in dielectrics result from three primary processes:

1. Ion migration losses
   (a) Dc conductivity losses
   (b) Ion jump and dipole relaxation losses
2. Ion vibration and deformation losses.
3. Electron polarization losses.

Of these electron polarization losses give rise to absorption and colour in the visible spectrum. Ion vibration and deformation losses become important in the infrared but are not a major concern for frequencies below about 10^{10} Hz. By far the major factor affecting the use of ceramic materials is the ion migration losses which tend to increase at low frequencies and as the temperature is raised.

The loss factor can be written in terms of the electrical conductivity,

$$\omega \varepsilon'' = \sigma = \omega \varepsilon' \tan \delta \qquad (15)$$

or
$$\tan\delta = \frac{\sigma}{2\pi f K' \varepsilon_0} = \frac{\sigma}{(8.85\times10^{-14})(2\pi f)K'} \qquad (16)$$

where conductivity is given in ohm-cm^{-1}. These conduction migration losses are normally small.

The total value for $\tan\delta$ is the sum of individual contributions already discussed. At lower frequencies conduction losses become important, at moderate frequencies ion jump and

dipole losses are most important, at intermediate frequencies dielectric losses are small, and at sufficiently high frequencies ion polarization effects give energy absorption.

For reasonably good insulators the conductivity increases exponentially with temperature. Consequently, for this process we would expect $\tan\delta$ to increase exponentially with temperature, as indicated in Eq. 16.

BIBLIOGRAPHY

1. W. D. Kingery, H. K. Bowen, D. R. Uhlmann, 'Introduction to Ceramics', Chap. 18, John Wiley and Sons, 1975.

2. J. B. Birks and J. Hart, editors, 'Progress in Dielectrics', p 151, Heywood and Company Ltd., 1961.

3. H. Fröhilich, 'Theory of Dielectrics', Oxford University Press, 1958.

4. C. P. Smyth, 'Dielectric Behaviour and Structure', McGraw-Hill Book Company, 1955.

5. C. J. F. Böttcher, 'Theory of Electric Polarisation', Elsevier Publishing Company, 1952.